Atmos. Chem. Phys., 24, 5199–5219, 2024
https://doi.org/10.5194/acp-24-5199-2024

Atmospheric Chemistry and Physics
Open Access
EGU

Research article

Dust storms from the Taklamakan Desert significantly darken snow surface on surrounding mountains

Yuxuan Xing[1], Yang Chen[1], Shirui Yan[1], Xiaoyi Cao[1], Yong Zhou[2], Xueying Zhang[2], Tenglong Shi[3], Xiaoying Niu[1], Dongyou Wu[1], Jiecan Cui[4], Yue Zhou[1], Xin Wang[1], and Wei Pu[1]

[1]Key Laboratory for Semi-Arid Climate Change of the Ministry of Education, College of Atmospheric Sciences, Lanzhou University, Lanzhou 730000, China
[2]Aviation University of Air Force, Changchun 130022, China
[3]Henan Industrial Technology Academy of Spatial-Temporal Big Data, Henan University, Kaifeng 475004, China
[4]Zhejiang Development & Planning Institute, Hangzhou 310030, China

Correspondence: Wei Pu (puwei@lzu.edu.cn)

Received: 29 June 2023 – Discussion started: 5 September 2023
Revised: 24 February 2024 – Accepted: 12 March 2024 – Published: 3 May 2024

Abstract. The Taklamakan Desert (TD) is a major source of mineral dust emissions into the atmosphere. These dust particles have the ability to darken the surface of snow on the surrounding high mountains after deposition, significantly impacting the regional radiation balance. However, previous field measurements have been unable to capture the effects of severe dust storms accurately, and their representation on regional scales has been inadequate. In this study, we propose a modified remote-sensing approach that combines data from the Moderate Resolution Imaging Spectroradiometer (MODIS) satellite and simulations from the Snow, Ice, and Aerosol Radiative (SNICAR) model. This approach allows us to detect and analyze the substantial snow darkening resulting from dust storm deposition. We focus on three typical dust events originating from the Taklamakan Desert and observe significant snow darkening over an area of ~ 2160, ~ 610, and $\sim 640\,\mathrm{km}^2$ in the Tien Shan, Kunlun, and Qilian mountains, respectively. Our findings reveal that the impact of dust storms extends beyond the local high mountains, reaching mountains located approximately 1000 km away from the source. Furthermore, we observe that dust storms not only darken the snowpack during the spring but also in the summer and autumn seasons, leading to increased absorption of solar radiation. Specifically, the snow albedo reduction (radiative forcing) triggered by severe dust deposition is up to 0.028–0.079 (11–31.5 $\mathrm{W\,m^{-2}}$), 0.088–0.136 (31–49 $\mathrm{W\,m^{-2}}$), and 0.092–0.153 (22–38 $\mathrm{W\,m^{-2}}$) across the Tien Shan, Kunlun, and Qilian mountains, respectively. This further contributes to the aging of the snow, as evidenced by the growth of snow grain size. Comparatively, the impact of persistent but relatively slow dust deposition over several months during non-event periods is significantly lower than that of individual dust events. This highlights the necessity of giving more attention to the influence of extreme events on the regional radiation balance. This study provides a deeper understanding of how a single dust event can affect the extensive snowpack and demonstrates the potential of employing satellite remote sensing to monitor large-scale snow darkening.

Published by Copernicus Publications on behalf of the European Geosciences Union.

1 Introduction

High Mountain Asia (HMA), which includes the Tibetan Plateau (TP) and surrounding mountain ranges, holds the largest amount of glaciers and snow outside of the poles. This region is informally known as the "Third Pole" and the "Asian Water Tower" (Yao et al., 2012, 2019) because of its extreme importance as a freshwater source, with approximately 1 billion people relying on the water and hydropower that the glaciers and snow across HMA regularly provide (Immerzeel and Bierkens, 2012; Mishra et al., 2018). The snow-covered area of HMA is a highly reflective natural surface that has a significant impact on the regional radiation balance (Cohen and Rind, 1991; Painter et al., 2012). Previous satellite and ground-based observations have demonstrated that the mass and extent of the snow cover across HMA are rapidly declining owing to recent global warming (Bormann et al., 2018; Notarnicola, 2020; Pulliainen et al., 2020). Furthermore, growing evidence has indicated that light-absorbing particles (LAPs) (Arun et al., 2019, 2021a, b; Chaubey et al., 2010; Gogoi et al., 2018, 2021a, b; Thakur et al., 2021), such as mineral dust and black carbon (BC), can induce a snow darkening effect when they are deposited on the snow surface (Wang et al., 2013; Qian et al., 2015; Dang et al., 2017; Huang et al., 2022; Niu et al., 2022; Réveillet et al., 2022; Shi et al., 2022c). This snow darkening effect increases solar absorption and decreases snow albedo, resulting in enhanced snowmelt (Hadley and Kirchstetter, 2012; Dumont et al., 2014; He et al., 2017, 2018; Pu et al., 2017; Shi et al., 2021, 2022a, b; Cordero et al., 2022) and an accelerated transformation of ice and snow into liquid water in the Asian Water Tower (Yao et al., 2022). Consequently, the snow darkening effect plays a critical role in snow decline across HMA, thereby perturbing the climate system and impacting hydrological cycles (Kraaijenbrink et al., 2017, 2021; Sang et al., 2019; Shi et al., 2019; Zhang et al., 2020; Y. Zhang et al., 2021; Roychoudhury et al., 2022; Yang et al., 2022).

The Taklamakan Desert (TD) in southwestern Xinjiang, northwest China, is the second-largest shifting sand desert on earth and accounts for 42 % of all dust emissions in East Asia (Chen et al., 2017b). Approximately 70.54 Tg of dust is emitted into the atmosphere annually, with the most intense dust events occurring in spring (Chen et al., 2017b). The dust in the Tarim Basin is predominantly redeposited onto nearby regions owing to the surrounding high mountains (Qiu et al., 2001; Sun et al., 2001; Shao and Dong, 2006). When the dust is uplifted above 4 km altitude, it may eventually settle on the snow surfaces across the surrounding high mountains, such as the Tien Shan and Kunlun mountains, and subsequently induce a snow darkening effect (Ge et al., 2014; Jia et al., 2015; Yuan et al., 2018). Furthermore, this dust is also transported eastward beyond the Tarim Basin and can be transported all the way to the Qilian Mountains via the westerly winds during spring and summer, thereby inducing a snow darkening effect in this distal region to the east of the TD (Dong et al., 2020; Han et al., 2022). Therefore, TD dust may have a profound effect on the regional radiative balance by darkening the snow across the high mountains surrounding the TD. This effect may subsequently accelerate snow melting and affect water resources for the 30+ million people living in the Xinjiang and Gansu provinces of China (Mishra et al., 2021).

Numerous field measurements have been undertaken in recent decades to investigate the dust content of snow/glaciers across the high mountains surrounding the TD, with measured dust contents generally varying from 1.4 to 110 $\mu g\,g^{-1}$ (Wake et al., 1994; Dong et al., 2009, 2014; Wu et al., 2010; Ming et al., 2016; Xu et al., 2016; Schmale et al., 2017; Zhang et al., 2018; X. Zhang et al., 2021; Wang et al., 2019; Li et al., 2021, 2022). This abundance of dust particles has been found to induce a significant snow darkening effect across the high-mountain snowpack, thereby increasing its associated radiative forcing to 25.8–65.7 $W\,m^{-2}$. Furthermore, the estimated natural dust-induced snow darkening effect can be equivalent to that induced by BC, particularly during intense springtime dust events (Sarangi et al., 2020; X. Zhang et al., 2021). These findings effectively highlight the significance of the TD dust-induced snow darkening effect across the surrounding high mountains. In spite of these invaluable in situ findings, ground-based observations are poorly represented at the regional scale owing to limited spatial coverage and temporal discontinuity (Arun et al., 2019). Furthermore, these previous field measurements may not be able to capture severe dust emission and loading events, which are more likely to induce snow darkening than common dry and wet deposition processes (Dumont et al., 2020; Pu et al., 2021; Baladima et al., 2022).

Satellite remote sensing offers an effective way to overcome the limitations of ground-based measurements by providing a more comprehensive understanding of the LAP-induced impact on the regional radiative forcing of the snowpack (Skiles et al., 2018a). For example, Painter et al. (2012) found that instantaneous LAP-induced radiative forcing can exceed 250 $W\,m^{-2}$ in the Hindu Kush Himalaya region via an analysis of Moderate Resolution Imaging Spectroradiometer (MODIS) satellite data. Sarangi et al. (2020) further revealed that dust is the primary factor responsible for high-altitude snow darkening in the Hindu Kush Himalaya region. Similarly, severe dust events from the Sahara can deposit dust on the snowpack across the European Alps and Caucasus Mountains (Di Mauro et al., 2015; Dumont et al., 2020), with this deposition inducing a radiative forcing of up to 153 $W\,m^{-2}$ based on satellite retrievals in Europe. Dust deposition has also induced extensive snow darkening across the Upper Colorado River basin in North America, particularly during extreme dust events (Skiles and Painter, 2016; Skiles et al., 2018b; Painter et al., 2017). These studies have demonstrated the effectiveness of employing satellite remote sensing to estimate the dust content of the snowpack and its

associated radiative forcing. However, detection of natural dust deposition on the snow surfaces across high mountains surrounding the TD is still limited.

Here we investigate the impact of dust storms on snow albedo reduction and radiative forcing across the high mountains surrounding the TD. We first capture three typical dust events that induced snow darkening in the Tien Shan, Kunlun, and Qilian mountains, respectively. Next, we utilize MODIS satellite data and the Snow, Ice, and Aerosol Radiative (SNICAR) model to retrieve the dust content of the snowpack. We then capture three typical dust events that induced snow darkening in the Tien Shan, Kunlun, and Qilian mountains, respectively. Finally, we analyze the spatial and altitudinal variations in dust-induced snow darkening and compare our retrievals with field measurements. Through remote sensing observations, we aim to provide a new view of the darkening effect of natural desert dust on the snowpack of the high mountains surrounding the TD.

2 Methodology

2.1 Remote-sensing data

We accessed two MODIS datasets, the surface reflectance (MOD09GA: https://earthdata.nasa.gov, last access: 19 April 2024); 500×500 m resolution) and aerosol optical depth (AOD; MCD19A2), to evaluate the impact of dust on snow albedo. MOD09GA is the daily surface reflectance product after the atmospheric correction from the Terra satellite, which provides the reflectance data for seven bands (band 1, 620–670 nm; band 2, 841–876 nm; band 3, 459–479 nm; band 4, 545–565 nm; band 5, 1230–1250 nm; band 6, 1628–1652 nm; and band 7, 2105–2155 nm). Previous studies have indicated that the MODIS sensor on Terra is not affected by saturation on bright snow surfaces. As a result, it has the capability of detecting changes in reflectance in the visible (VIS) bands caused by dust in snow (Painter et al., 2012; Pu et al., 2019). Additionally, we used the updated MODIS aerosol optical depth product MCD19A2, based on the MAIAC algorithm, to assess the AOD levels during dust events. This is a combined product of Terra/Aqua with a spatiotemporal resolution of 1 km, which was resampled to 500 m resolution using GEE (https://earthengine.google.com/, last access: 19 April 2024).

The daily averaged downward shortwave flux was obtained from the NASA Clouds and the Earth's Radiant Energy System (CERES; $1^\circ \times 1^\circ$ resolution; https://ceres.larc.nasa.gov, last access: 19 April 2024). The CERES data products take advantage of the synergy between collocated CERES instruments and spectral imagers, such as MODIS (Terra and Aqua) and the Visual Infrared Imaging Radiometer Suite (S-NPP and NOAA-20). We used the downward shortwave flux to estimate the daily averaged radiative forcing that was due to dust deposition on the snowpack. The Cloud-Aerosol Lidar with Orthogonal Polarization (CALIOP/CALIPSO) provided by NASA is able to detect the type and height of aerosols in the atmosphere (Huang et al., 2007; Han et al., 2022) and can therefore be used to identify the movement of dust storms over the high mountains surrounding the TD.

The Shuttle Radar Topography Mission (SRTM) digital elevation data, which have a 90 m spatial resolution, were provided by NASA and downloaded from Google Earth Engine (https://earthengine.google.com, last access: 19 April 2024). These data were used to correct the influence of topography on surface reflectance.

2.2 Snow depth and wind data

The snow depth data were provided by NASA and accessed from the Modern-Era Retrospective Analysis for Research and Applications, version 2 (MERRA-2; https://gmao.gsfc.nasa.gov/, last access: 19 April 2024). The MERRA-2 snow depth product was selected because it has better accuracy than those from ERA-Interim, JJA-55, and ERA5 across HMA (Orsolini et al., 2019). The wind field data were obtained from the European Centre for Medium-Range Weather Forecasts (ECMWF) Reanalysis version 5 (ERA5; https://www.ecmwf.int/, last access: 19 April 2024) owing to its superior performance in terms of its high spatial resolution and longer time span compared with other products (Copernicus Climate Change Service, 2017). Here, we used ERA5 wind data at 700 hPa to describe the atmospheric circulation during the analyzed dust storms.

2.3 Radiative transfer model

The SNICAR model is a two-stream radiative transfer model (Flanner et al., 2007, 2009) that has been widely used to simulate the spectral albedo of LAP-contaminated snow (Sarangi et al., 2019; Chen et al., 2021). The model includes snow properties, such as snow depth and effective radius, and accounts for the incident radiation at the surface and its spectral distribution, solar zenith angle, as well as the type and concentration of LAPs in the snowpack. In this study, dust optical parameters are taken from SNICAR defaults, where the refractive index is $1.56 + 0.0038i$ at 0.63 µm (Patterson et al., 1981; Flanner et al., 2007). In addition, a diameter bin of 0.1–1 µm was selected according to the previous observations from Taklamakan Desert (Okada and Kai, 2004). Furthermore, a single-layer snowpack model was adopted in our study, in line with Cui et al. (2021), since the snow darkening effect typically pertains to surface snow. This simplification minimally affects the retrieval of LAPs from the surface snow, despite the complex multilayer structure of natural snowpacks.

The Santa Barbara DISORT Atmospheric Radiative Transfer (SBDART) model is one of the most widely used models for simulating the surface solar irradiance in clear- and cloudy-sky conditions (Ricchiazzi et al., 1998). The SB-

DART model includes standard atmospheric models, cloud models, extraterrestrial source spectra, gas absorption models, standard aerosol models, and surface models. Here, we used the SBDART model to calculate the spectral surface solar irradiance following the approach of Cui et al. (2021). In this study, the cloud-free condition was set in SBDART according to the MODIS images.

2.4 Terrain correction

The high mountains surrounding the TD have a complex terrain, such that the local solar zenith angle (β) may differ from the MODIS-derived solar zenith angle (θ_0). Therefore, the topographic correction method should be used to derive β (Teillet et al., 1982; Negi and Kokhanovsky, 2011):

$$\cos\beta = \cos\theta_0 \cos\theta_T + \sin\theta_0 \sin\theta_T \cos(\phi_0 - \phi_T)\,, \quad (1)$$

where ϕ_0 is the solar azimuth angle from MODIS, and θ_T and ϕ_T are the surface slope and aspect from SRTM, respectively. We then replace θ_0 with β in subsequent satellite retrievals.

2.5 Snow property retrieval

The dust-contaminated spectral snow albedo is determined based on the dust content, snow grain size, snow depth, and solar zenith angle (Wiscombe and Warren, 1980). The dust content and snow depth primarily impact the snow albedo in the ultraviolet (UV) and VIS wavelengths, with a much smaller effect on snow albedo in the near infrared (NIR) wavelengths (Figs. 1 and S1 in the Supplement). Conversely, the snow grain size and solar zenith angle primarily impact the snow albedo in the NIR wavelengths. The solar zenith angle and snow depth data are from MODIS Terra and MERRA-2, respectively. We used the SNICAR model to derive the quantitative snow grain size and dust content from the MODIS data. Then the SBDART model was combined to estimate the dust-induced snow albedo reduction and radiative forcing. Figure 2 shows the flowchart of the overall retrieval process.

The Snow-Covered Area and Grain size (SCAG) model is a spectral unmixing method that is widely used for identifying snow-cover fraction (SCF) and snow optical effective radius (R_{eff}), especially in complex mountain terrains (Painter et al., 2009, 2012; Rittger et al., 2013). The SCAG model retrieves the SCF and R_{eff} using all seven bands of the MODIS reflectance data, which span the VIS to NIR range. It does not consider the impact of LAPs. However, in our study, the dust content in snow is extremely high, which will significantly reduce the VIS snow albedo in MODIS bands 1, 3, and 4 (Fig. 1). So, the SCAG model will introduce a large bias in the resultant SCF and R_{eff} retrievals. Furthermore, the reflectance of fine-grained dirty snow has been compared with that of pure coarse-grained snow at short-wave infrared wavelengths, which include bands 6 and 7 (Bair et al., 2020). The extremely high dust content in this study

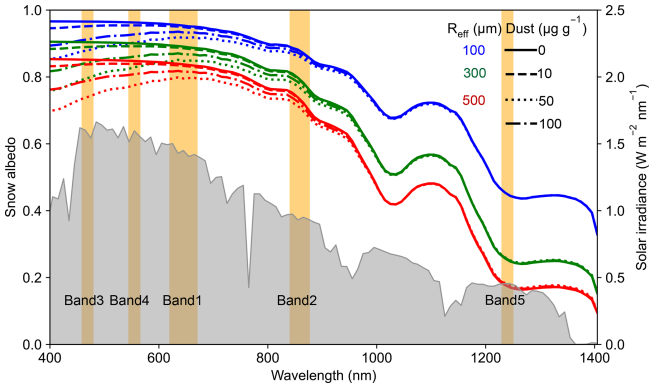

Figure 1. Snow albedo spectra for different snow optical effective radii (R_{eff}) and dust contents that were simulated using the SNICAR model. The orange bars denote MODIS bands and the gray region represents the typical solar irradiance in HMA.

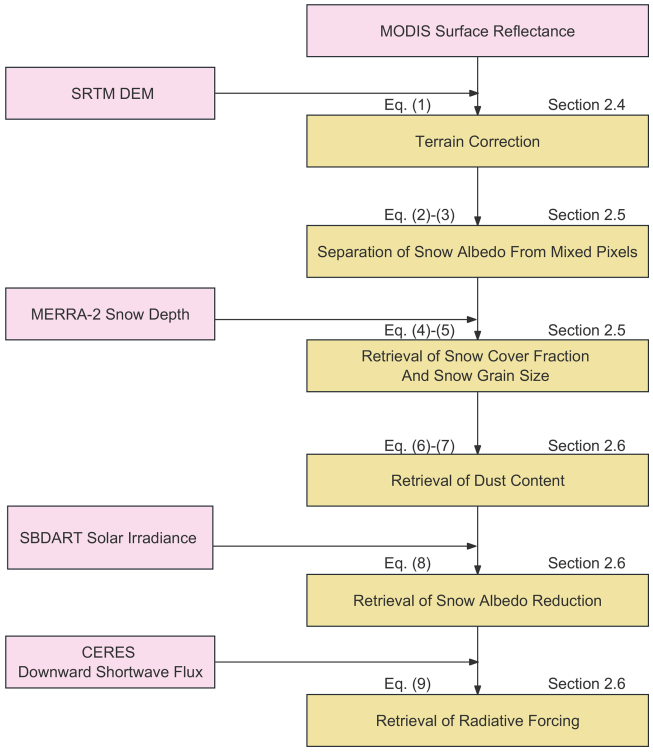

Figure 2. Flowchart illustrating the step-by-step retrieval of dust content as well as the associated snow albedo reduction and radiative forcing. The pink boxes denote the external input data, while the yellow boxes are used for calculations in this study.

therefore means that the reflectance in MODIS bands 6 and 7 is not appropriate for snow property retrieval. Instead, we used the reflectance data in MODIS bands 2 and 5 to unmix the surface reflectance to derive SCF and R_{eff} (Fig. 2), similar to the approach in Painter et al. (2009). The surface reflectance at band i ($R^{\mathrm{MODIS}}_{\mathrm{band}\ i}$) can be expressed as follows

(Cui et al., 2021, 2023):

$$R_{\text{band } i}^{\text{MODIS}} = \frac{E_{\text{band } i} \times \text{SCF} \times R_{\text{band } i}^{\text{MODIS, snow}} + E_{\text{band } i} \times (1-\text{SCF}) \times R_{\text{band } i}^{\text{soil}}}{E_{\text{band } i}} = \text{SCF} \times R_{\text{band } i}^{\text{MODIS, snow}} + (1-\text{SCF}) \times R_{\text{band } i}^{\text{soil}}, \quad (2)$$

where $R_{\text{band } i}^{\text{MODIS, snow}}$ and $R_{\text{band } i}^{\text{soil}}$ represent the snow and soil reflectances at band i, respectively, with $R_{\text{band } i}^{\text{soil}}$ taken from Siegmund and Menz (2005), and $E_{\text{band } i}$ is the solar irradiance at band i. The snow reflectance at band i ($R_{\text{band } i}^{\text{MODIS, snow}}$) can be expressed as

$$R_{\text{band } i}^{\text{MODIS, snow}} = \left(\frac{R_{\text{band } i}^{\text{MODIS}} - (1-\text{SCF}) \times R_{\text{band } i}^{\text{soil}}}{\text{SCF}} \right). \quad (3)$$

We then fit the SNICAR-simulated snow reflectance to the MODIS-derived snow reflectance, which is expressed as either

$$\text{RMSE} = \left(\frac{1}{2} \left(a \times \left(R_{\text{band 2}}^{\text{SNICAR, snow}} - R_{\text{band 2}}^{\text{MODIS, snow}} \right)^2 + \left(R_{\text{band 5}}^{\text{SNICAR, snow}} - R_{\text{band 5}}^{\text{MODIS, snow}} \right)^2 \right) \right)^{\frac{1}{2}} \quad (4)$$

or

$$\text{RMSE} = \frac{1}{2} \left(a \times \left(R_{\text{band 2}}^{\text{SNICAR, snow}} - \left(\frac{R_{\text{band 2}}^{\text{MODIS}} - (1-\text{SCF}) \times R_{\text{band 2}}^{\text{soil}}}{\text{SCF}} \right) \right)^2 + \left(R_{\text{band 5}}^{\text{SNICAR, snow}} - \left(\frac{R_{\text{band 5}}^{\text{MODIS}} - (1-\text{SCF}) \times R_{\text{band 5}}^{\text{soil}}}{\text{SCF}} \right) \right)^2 \right)^{\frac{1}{2}}, \quad (5)$$

where RMSE is the root mean square error, $R_{\text{band } i}^{\text{SNICAR, snow}}$ is the SNICAR-simulated snow reflectance at band i (which is dependent on the R_{eff} and solar zenith angle, where the solar zenith angle is derived from the MODIS data), and a is an empirical coefficient (0.1–1 range). In this study, a was set to 0.1 to reduce the interference of dust on the snow property retrieval because a high dust content can influence the snow albedo at band 2 (Fig. 1). We can then derive SCF and R_{eff} by minimizing the RMSE (Painter et al., 2009).

2.6 Dust content and snow albedo reduction retrieval

We fit the SNICAR-simulated snow reflectance to the MODIS-derived snow reflectance in bands 3 and 4, which are the most sensitive to the dust content in snow, following Pu et al. (2019) and Cui et al. (2021), which are expressed as either

$$\text{RMSE} = \frac{1}{2} \left(\left(R_{\text{band 3}}^{\text{SNICAR, snow}} - R_{\text{band 3}}^{\text{MODIS, snow}} \right)^2 + \left(R_{\text{band 4}}^{\text{SNICAR, snow}} - R_{\text{band 4}}^{\text{MODIS, snow}} \right)^2 \right)^{\frac{1}{2}} \quad (6)$$

or

$$\text{RMSE} = \left(\frac{1}{2} \left(\left(R_{\text{band 3}}^{\text{SNICAR, snow}} - \left(\frac{R_{\text{band 3}}^{\text{MODIS}} - (1-\text{SCF}) \times R_{\text{band 3}}^{\text{soil}}}{\text{SCF}} \right) \right)^2 + \left(R_{\text{band 4}}^{\text{SNICAR, snow}} - \left(\frac{R_{\text{band 4}}^{\text{MODIS}} - (1-\text{SCF}) \times R_{\text{band 4}}^{\text{soil}}}{\text{SCF}} \right) \right)^2 \right) \right)^{\frac{1}{2}}, \quad (7)$$

where $R_{\text{band 3}}^{\text{SNICAR, snow}}$ is a function of four factors: dust content, R_{eff}, snow depth, and solar zenith angle. The latter three factors have been derived, leaving the dust content as the only unknown. Therefore, the dust content can be retrieved by minimizing Eq. (7). We assume that the derived dust content in this study accounts for the total light absorption by all of the LAPs that are present in the snowpack. This is because our study area is close to the Taklamakan Desert (TD), where large amounts of dust accumulate on the snow surface annually. In contrast, anthropogenic activities and biomass burning are rare, resulting in limited depositions of black carbon (BC) and organic carbon (OC) (Fig. S8). Observations from snow and atmosphere have confirmed this phenomenon (Wake et al., 1994; Huang et al., 2007). Therefore, our assumption is plausible.

The dust-induced broadband albedo reduction ($\Delta\alpha$) can then be calculated as follows:

$$\Delta\alpha = \frac{\sum_{\lambda=300\,\text{nm}}^{\lambda=2500\,\text{nm}} E_\lambda \cdot \left(R_\lambda^{\text{SNICAR, pure-snow}} - R_\lambda^{\text{SNICAR, snow}} \right) \cdot \Delta\lambda}{\sum_{\lambda=300\,\text{nm}}^{\lambda=2500\,\text{nm}} E_\lambda \cdot \Delta\lambda}, \quad (8)$$

where $R_\lambda^{\text{SNICAR, pure-snow}}$ and $R_\lambda^{\text{SNICAR, snow}}$ are the SNICAR-simulated pure and polluted snow albedo using the snow grain size and dust content retrieved above, solar zenith angle from MODIS, and snow depth from MERRA2, respectively. E_λ represents the spectral solar irradiance at wavelength λ simulated from the SBDART model, $\Delta\lambda$ is 10 nm, and $R_\lambda^{\text{SNICAR, pure-snow}}$ and $R_\lambda^{\text{SNICAR, snow}}$ are the SNICAR-simulated pure and polluted snow albedo, respectively. The spectral irradiance from SBDART is only used for integrating the spectral MODIS albedo to achieve broadband albedo. Thus, the uncertainty in solar irradiance from the assumed atmospheric properties has limited influence on the retrieval of snow albedo reduction (Cui et al., 2021).

The dust-induced radiative forcing (RF) is calculated as follows:

$$\text{RF} = \Delta\alpha \cdot \text{SW}, \quad (9)$$

where SW is the downward shortwave flux, which is obtained from CERES.

The in situ dust content was not measured to verify the MODIS retrievals because of the challenging geographical conditions surrounding the TD. Nevertheless,

Cui et al. (2021) verified a similar retrieval method across the Northern Hemisphere. They considered that the accuracy of MODIS surface reflectance is typically $\pm(0.005 + 0.05 \times \text{reflectance})$ under conditions where aerosol optical depth (AOD) is less than 5.0 and solar zenith angle is less than 75°, as stated in the MODIS Surface Reflectance user's guide (Collection 6; https://modis.gsfc.nasa.gov/data/dataprod/mod09.php; last access: 19 January 2024). In addition, the bias for snow grain size retrieval was assumed to be 30 % according to the studies of Pu et al. (2019) and Wang et al. (2017). These biases led to an overall uncertainty ranging from 10 % to 110 % in the retrieval of LAPs across the Northern Hemisphere. The study revealed that uncertainty decreased as LAP concentration increased, with reported uncertainties dropping to below approximately 30 % in regions of high pollution, such as northeast China. In our study, the snowpack was also significantly polluted due to severe dust depositions, leading us to consider a retrieval uncertainty of 30 % for LAPs, in alignment with the findings of Cui et al. (2021). Then, the overall lower bound and upper bound of the uncertainty value of snow albedo reduction retrieval was calculated and will be discussed in the following section. Moreover, we utilized the LAPs and the corresponding albedo reduction retrieved at the local time of 10:30 (the time of the MODIS Terra satellite overpass) as the proxy for daily averages following Painter et al. (2012). This approximation was reasonable, given that the content of LAPs exhibited little variation over a diurnal cycle (Painter et al., 2009; Zege et al., 2011). The variation in snow albedo throughout the day was primarily attributed to changes in the solar zenith angle (Fig. S1). Since the solar zenith angle predominantly influences snow albedo in NIR, with little impact on the VIS, the diurnal variation in LAP-induced snow albedo reduction was also considered limited.

As noted above, the snow albedo reduction is mainly dependent on the dust content, R_{eff}, snow depth, and solar zenith angle. The R_{eff} and snow depth can be categorized as snow properties. We compared the dust content, snow properties, and solar zenith angle to discuss their contributions to the spatial variations in snow albedo reduction (Pu et al., 2019; Cui et al., 2021). The Supplement contains a thorough derivation of this method.

3 Results

3.1 Remote sensing of the snow darkening effect across the high mountains surrounding the TD

The TD is located in the northern part of HMA and is surrounded by some of the highest mountain ranges on earth, including the Kunlun, Tien Shan, and Pamir mountains (Fig. 3a and b). The TD region emits vast amounts of dust particles into the atmosphere each year, particularly during the spring and summer (Wang et al., 2008; Chen et al., 2013, 2017a; Kang et al., 2016; Wu et al., 2021; Tang et al., 2022). This phenomenon is confirmed by the high AOD levels at 550 nm from March to August (Fig. 3c). A significant amount of this dust is ultimately redeposited across the Tarim Basin and the surrounding mountains. The Tien Shan and Kunlun mountains are two regions that experience high levels of dust deposition owing to the local topography and atmospheric circulation patterns (Fig. 3d) (Huang et al., 2007, 2014; Ge et al., 2014; Dong et al., 2022). Therefore, we selected two typical cases to demonstrate the snow darkening effect across the mountains surrounding the TD, a springtime dust event across the Tien Shan and a summertime dust event across the Kunlun Mountains.

3.1.1 Dust-induced snow darkening across the Tien Shan

A significant dust storm occurred across the TD region on 18–22 May 2019 (Figs. 4 and S2). The 21 May 2019 Terra/MODIS satellite image (Fig. 4b) showed that the dust plumes had spread to the north and east owing to an upper anticyclone system in the Tarim Basin (Fig. 4h). Some dust particles were uplifted to > 4 km altitude, as shown in the CALIPSO aerosol vertical profiles (Fig. 4j and k). These dust particles were then transported to the snow-covered high-elevation areas of the Tien Shan, as illustrated in the MODIS AOD images (Fig. 4h and i). Dust plumes were also observed in a satellite image that spanned the broadly snow-covered central Tien Shan (Fig. 4e), and the snow appeared to darken in the 22 May 2019 Terra/MODIS satellite image that was acquired under the first clear-sky conditions after this severe dust event. However, the snow was much whiter prior to the passage of this dust storm, as shown in Fig. 4d and f. Figure 4g further illustrates changes in the surface reflectance of the snow-covered areas, providing a more intuitive influence of dust deposition on the snow physical properties. The reflectance was around 0.8 in the VIS spectrum on 15 May 2019, but it quickly decreased to < 0.7 on 22 May 2019, after the passage of the dust plumes. The reduction in VIS wavelengths was up to > 0.1 during this short time interval. These observations show that the dust plumes from the TD can significantly darken the snowpack across the Tien Shan through heavy dust deposition. Furthermore, the progression of air-temperature-induced snow aging cannot effectively explain this phenomenon. This result is consistent with previous satellite observations over the Himalayas (Gautam et al., 2013).

We also derived the spectral snow albedo and retrieved several parameters to quantitatively assess the impact of this dust deposition on snow darkening. The SNICAR-simulated spectral snow albedo (solid lines) and MODIS-derived 5-band snow albedo (dots) in Fig. 5a are averaged over the area in Fig. 5c. These results demonstrate an agreement of > 95 %, thereby indicating the reliability of our retrievals. The spectral snow albedo reductions on 15 and 22 May 2019 are shown in Fig. 5b. There were significant increases in the

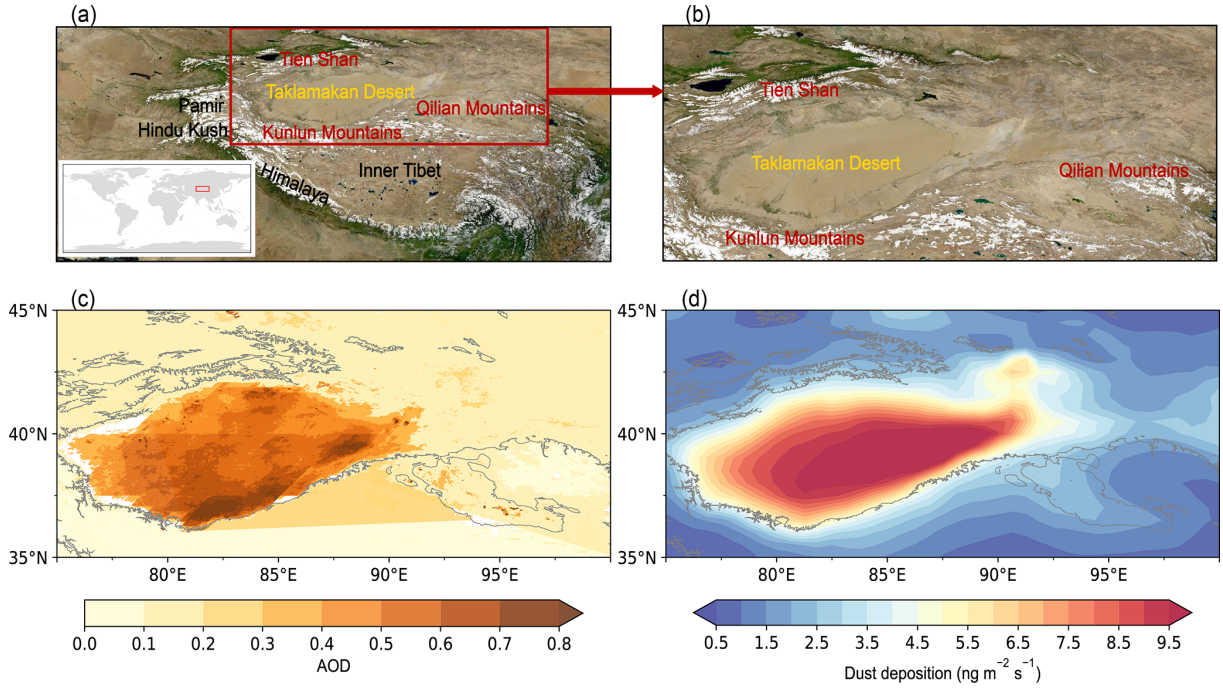

Figure 3. Mountain ranges surrounding the Taklamakan Desert, as well as AOD and dust deposition distributions across the Taklamakan Desert and surrounding region. Panels **(a)** and **(b)** show the geographic location of the Taklamakan Desert and surrounding mountains. Satellite images are from Terra/MODIS (https://worldview.earthdata.nasa.gov, last access: 19 April 2024). The red box defines the area in **(b)**. Shown also are the spatial distributions of the averaged **(c)** AOD and **(d)** dust deposition values, which were derived from MCD19A2 and MERRA-2 during the March to August 2019 period.

albedo reductions as the wavelength decreased, particularly on 22 May 2019, which is consistent with theoretical simulations of the dust-induced snow darkening effect (Fig. 1). However, the spectral curve differed from the BC-induced results in the anthropogenically influenced areas of northeast China (Wang et al., 2017; Niu et al., 2022) and northwest China (Shi et al., 2020). Therefore, we indicate that the observed snow darkening in this study was mainly caused by natural dust emissions, as opposed to BC and organic carbon (OC) emissions from anthropogenic activities and/or biomass burning. There was a spectral snow albedo reduction of 0.02–0.08 in the VIS on 15 May 2019, which represents persistent but relatively low dust deposition during spring. However, the severe dust event caused a rapid increase in spectral snow albedo reduction to 0.045–0.18 in a matter of days. The approximate doubling of the albedo reduction indicates that the increase in the dust concentration was much greater than 100 % based on the nonlinear theory of the snow albedo feedback to the dust concentration (Fig. 1). This implies that it is important to consider both the frequency and intensity of dust events when examining their impact on snow albedo. Similar phenomena that were induced by catastrophic wildfire events have been observed in the snowpack across New Zealand (Pu et al., 2021). These results suggest that extreme events may reflect the more pronounced impact of climate warming on our planet (Liang et al., 2021; Gui et al., 2022). Therefore, it is important to pay more attention to extreme events, rather than just conducting either annual or monthly averaged analyses, to fully capture the influence of climate change on snow albedo.

Figure 5c and d illustrate the spatial distributions of the dust concentration in the snowpack on 15 and 22 May 2019, respectively. There was a sharp increase in the dust content from 2–55 to 42–192 µg g^{-1} ($\sim$ 2.67-fold increase) following the severe dust event, with the lower elevations possessing higher dust concentrations and greater dust content increases (Figs. 5d, e, and S3). Snow darkening was observed across all of the snow-covered areas ($>$ 2100 km^2), including the summits, thereby highlighting the extensive influence of this severe dust event across the central Tien Shan. Furthermore, these results demonstrate the capability and effectiveness of employing satellite remote sensing to observe or monitor large-scale snow darkening. The dust-induced broadband snow albedo reductions and radiative forcing are shown in Fig. 5f–k, with observed spatial patterns that are largely similar to the dust content distributions. The snow albedo reduction increased by 0.008–0.052, with an observed increase from 0.002–0.032 on 15 May to 0.028–0.079 on 22 May. The radiative forcing increased by 2.5–20.5 W m^{-2}, with an observed increase from 0.5–12.5 W m^{-2} on 15 May to 11–31.5 W m^{-2} on 22 May (Fig. S4). Both the snow albedo reduction and radiative forcing increased by a factor of $\sim$ 2.39,

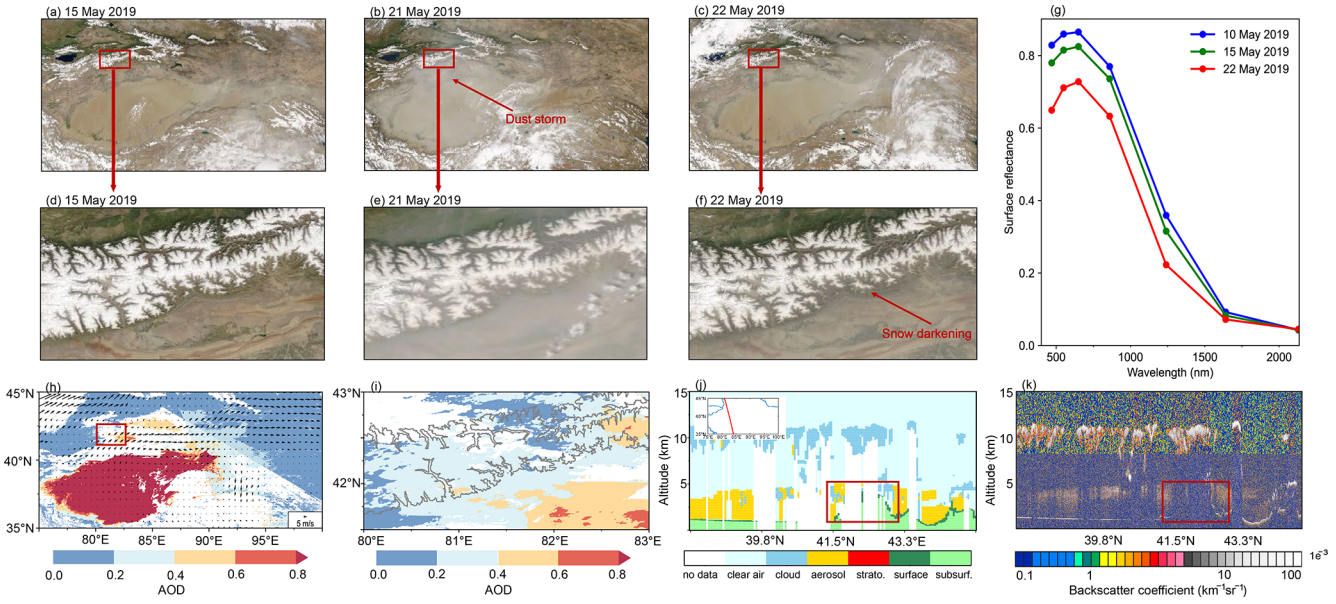

Figure 4. Satellite observations during the 18–22 May 2019 severe dust event across the Tien Shan. Panels **(a)** and **(d)** are Terra/MODIS satellite true-color images acquired on 15 May 2019, prior to the dust storm. Panels **(b)** and **(e)** are Terra/MODIS satellite images acquired on 21 May 2019, with the dust storm transport from the TD to the Tien Shan indicated by the red arrow in **(b)**. Panels **(c)** and **(f)** are Terra/MODIS satellite images acquired on 22 May 2019, with significant snow darkening observed across the Tien Shan after the dust storm. Satellite images **(a)**–**(f)** are from Terra/MODIS (https://worldview.earthdata.nasa.gov, last access: 19 April 2024). Panel **(g)** shows MOD09GA spectral surface reflectance across snow-covered areas on 10 May 2019 (blue), 15 May 2019 (green), and 22 May 2019 (red). Panel **(h)** is a MODIS AOD image acquired on 21 May 2019, with the ERA5 daily mean wind vector at 700 hPa overlain. Panel **(i)** is a MODIS AOD image across the Tien Shan acquired on 21 May 2019. Gray lines denote the 3000 m elevation contour. CALIPSO **(j)** vertical feature mask and **(k)** backscatter coefficient on 21 May 2019.

which directly reflects its significant impact on the regional radiation balance and climate (Dumont et al., 2020). Snow darkening can also accelerate snow aging by absorbing more shortwave radiation in a warming spring, as characterized by the R_{eff} growth (Fig. S3a, b, and c). Figure S5a–d show the overall uncertainty in snow albedo reduction retrieval in Tien Shan, with the uncertainty bounds averaging 24 % (−26 %) on 15 May and 22 % (−24 %) on 22 May, respectively. As the dust content increases, the uncertainty in the snow albedo reduction decreases.

3.1.2 Dust-induced snow darkening across the Kunlun Mountains

The Kunlun Mountains are located along the southern (northern) edge of the Tarim Basin (Tibetan Plateau). The northern slope of the central/west Kunlun Mountains directly faces the TD (Fig. 1a) and should have experienced the most severe dust-induced snow darkening. Similar conditions also exist across the Himalayas, where the south slope faces both the Thar Desert in India and the Middle East. We captured a typical dust storm event with associated dust deposition and snow darkening that occurred between 5 and 11 May 2020 along the northern slope of the Kunlun Mountains using MODIS satellite images (Fig. S6). The previously mentioned spring phenomenon is well known due to intense springtime dust emissions from the TD, whereas the summer phenomenon is usually overlooked. However, it has been shown that dust can more effectively cross the Kunlun Mountains during the summer months, with the potential to induce changes in atmospheric dynamics and thermal effects (Yuan et al., 2018). Therefore, we specifically chose a summer case to highlight snow darkening across the Kunlun Mountains.

A significant dust event that impacted the northern slope of the Kunlun Mountains occurred from 26 August to 8 September 2019 (Figs. 6b and S7). The Terra/MODIS satellite images on 5 September 2019 (Fig. 6b and e) show the accumulation of dust plumes along the southern edge of the Tarim Basin. In summer, the westerlies weaken and shift to the north, leading to more accumulation of dust locally instead of transporting it eastward (Chen et al., 2017b; Yuan et al., 2018). Furthermore, the enhanced sensible heat flux favors the southward transport of uplifted dust, leading to cyclonic convergence at the surface and anticyclonic divergence at the top of the troposphere above the TD (Fig. 6h). The synergistic effects of atmospheric dynamic and thermal forcing can cause the dust plumes to be uplifted to ∼ 5 km altitude (Fig. 6j and k). This uplift effectively facilitated the dust plume ascent to the snow-covered areas across the northern slope of the Kunlun Mountains (Fig. 6e and i). A com-

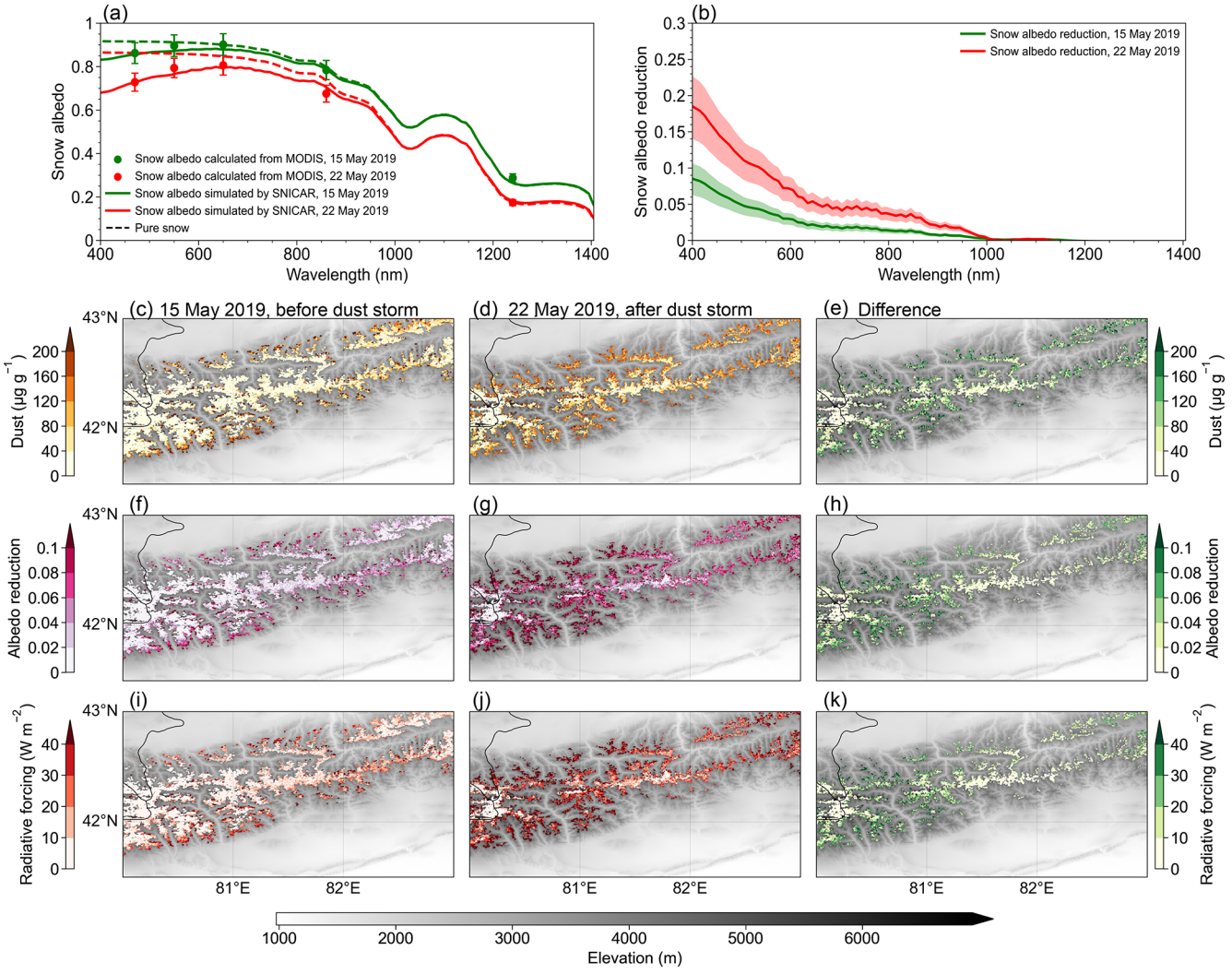

Figure 5. Panel **(a)** shows the averaged SNICAR-simulated spectral snow albedo (solid lines) and MODIS-derived five-band snow albedo (dots) for the region across the Tien Shan impacted by the 18–22 May 2019 severe dust event. Panel **(b)** shows the snow albedo reduction on 15 May 2019 (green) and 22 May 2019 (red). Shadings indicate the retrieval uncertainty. Spatial distributions of the average **(c, d)** dust, **(f, g)** albedo reduction, and **(i, j)** radiative forcing on 15 and 22 May 2019, respectively. Spatial distributions of the differences in **(e)** dust, **(h)** albedo reduction, and **(k)** radiative forcing between 15 and 22 May 2019. The background image in **(c)**–**(k)** is a grayscale topographic map of the Tien Shan.

parison of the MODIS images that were acquired on 23 August and 6 September 2019 highlighted snow darkening after this severe dust storm (Fig. 6d and f). The surface reflectance decreased by ~ 0.22 in the VIS spectrum, decreasing from 0.285 on 23 August to ~ 0.065 on 5 September. These observations indicate that this summertime dust event caused significant snow darkening across the Kunlun Mountains.

Figure 7 provides a more quantitative investigation of the impact of this severe dust event on the snowpack across the Kunlun Mountains, whereby a significant increase in dust content from 12–50 $\mu g\,g^{-1}$ on 23 August to 170–360 $\mu g\,g^{-1}$ on 6 September (~ 6.45-fold increase) is observed after this severe dust event (Fig. S8). The darkened snow-covered area spans $> 600\,km^2$, with a clear south–north gradient in the dust concentration distribution that is influenced by both the orientation and elevation of the mountains. This large dust deposition induced a 0.015–0.106 increase in snow albedo reduction, with an observed increase from 0.013–0.032 on 23 August to 0.088–0.136 on 6 September. There was also a substantial increase in radiative forcing of 4.1–37.5 $W\,m^{-2}$, with an observed increase from 3–11 $W\,m^{-2}$ on 23 August to 31–49 $W\,m^{-2}$ on 6 September (Fig. S4). Note that these increases in both the snow albedo reduction and radiative forcing are approximately two times larger than those observed over the Tien Shan (Figs. S3 and S8). These findings indicate accelerated snow aging, as evidenced by the faster

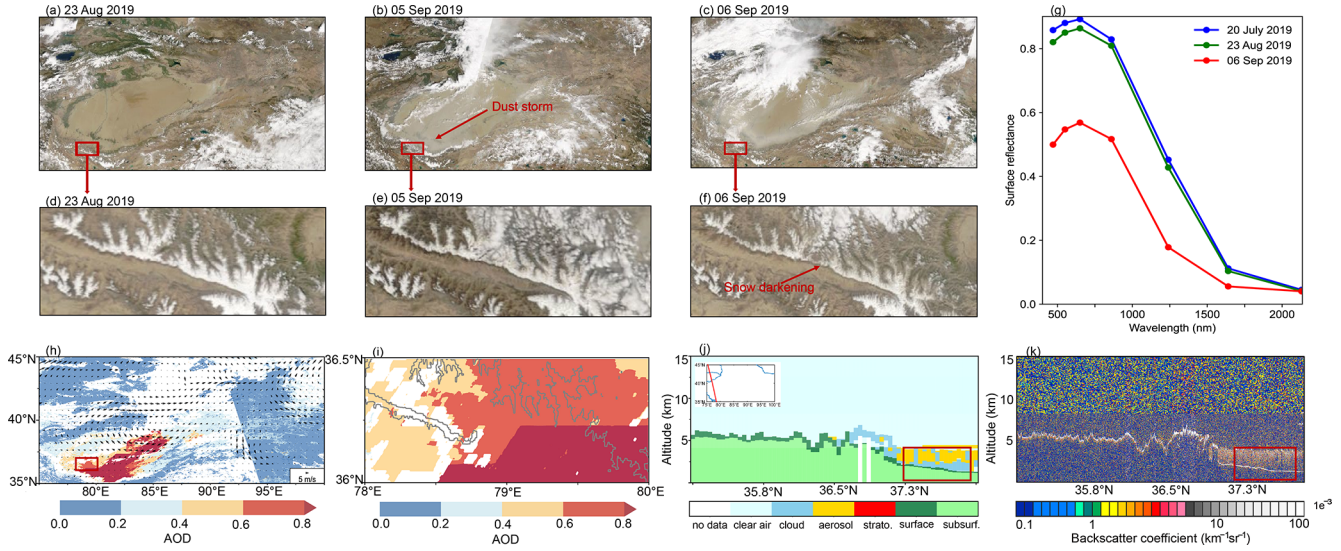

Figure 6. Satellite observations during the 26 August to 8 September 2019 dust storm across the Kunlun Mountains. Panels **(a)** and **(d)** are Terra/MODIS satellite true-color images acquired on 23 August 2019, prior to the dust storm. Panels **(b)** and **(e)** are Terra/MODIS satellite images acquired on 5 September 2019, with the dust storm transport from the TD to the Kunlun Mountains indicated by the red arrow in **(b)**. Panels **(c)** and **(f)** are Terra/MODIS satellite images acquired on 6 September 2019, with significant snow darkening across the Kunlun Mountains after the dust storm. Satellite images **(a)**–**(f)** are from Terra/MODIS (https://worldview.earthdata.nasa.gov, last access: 19 April 2024). Panel **(g)** shows MOD09GA spectral surface reflectance over the snow-covered areas on 20 July 2019 (blue), 23 August 2019 (green), and 6 September 2019 (red). Panel **(h)** is a MODIS AOD image acquired on 5 September 2019, with the ERA5 daily mean wind vector at 700 hPa overlain. Panel **(i)** is a MODIS AOD image across the Kunlun Mountains from 5 September 2019. Gray lines denote the 3000 m elevation contour. CALIPSO **(j)** vertical feature mask and **(k)** backscatter coefficient on 4 September 2019.

growth rate of the R_{eff} observed across the Kunlun Mountains (Fig. S9). Furthermore, Fig. S5e–h show the overall uncertainty in snow albedo reduction retrieval in Kunlun Mountains, with the uncertainty bounds averaging 23 % (−25 %) on 23 August and 7 % (−21 %) on 6 September, respectively. Notably, compared with the Tien Shan dust event described in Sect. 3.1.1, the Kunlun Mountains event demonstrates a more significant reduction in the uncertainty of snow albedo reduction as the dust content increases, especially in the upper bound of the uncertainty. This observation aligns with findings reported by Cui et al. (2021).

3.1.3 Snow darkening across the Qilian Mountains

Unlike the Tien Shan and Kunlun mountains, the Qilian Mountains are located approximately 1000 km east of the Tarim Basin. The Hexi Corridor, a narrow and relatively flat plain that lies between the high-elevation, inhospitable terrains of the Mongolian and Tibetan plateaus (see Fig. 3), is situated to the north of the Qilian Mountains. The unique terrain of the region results in TD dust plumes following a preferred transport route across the Hexi Corridor to East Asia (Zhang et al., 2008; Meng et al., 2018). These dust plumes are generally uplifted to >4 km altitude and entrained in the westerlies (Huang et al., 2008; Dong et al., 2014; Chen et al., 2022), thereby providing a means for dust deposition onto the snowpack across the Qilian Mountains.

Figure 8 illustrates a severe dust event that occurred from 2 to 4 November 2012 (Fig. S10), when abundant dust plumes were being transported across the narrow Hexi Corridor (Fig. 8b and h). The dust content was much more intense in this region, possessing AOD levels of up to >0.8. Furthermore, the CALIPSO observations indicated that the dust plumes were uplifted to ~ 10 km altitude (Fig. 8j and k), thereby allowing some dust particles to cross over the northern slopes of the Qilian Mountains and spread across its western extent (Fig. 8e and i). The average reflectance in the VIS spectrum was stable at around 0.7–0.8 across the snow-covered areas about a week before the severe dust event but then significantly decreased to 0.6–0.7 owing to heavy dust deposition.

Figure 9 presents the quantitative satellite-derived results, which highlight a rapid increase in dust content from 110–228 to 194–360 $\mu g\,g^{-1}$ (~ 1.53-fold increase) that spanned a snow-covered area of $>630\,km^2$ (Fig. 9f, g, and h). This significant increase in dust content led to a considerable increase in snow albedo reduction (radiative forcing) of 0.018–0.067 (3–16 $W\,m^{-2}$), which increased from 0.042–0.076 (11–20 $W\,m^{-2}$) on 1 November 2012 to 0.092–0.153 (22–38 $W\,m^{-2}$) on 4 November 2012 (Fig. S4). This >1.5-fold increase in snow albedo reduction (radiative forcing) was not solely due to the deposition of dust (Fig. S11). Accelerated snow aging, which was observed from the enhanced R_{eff}

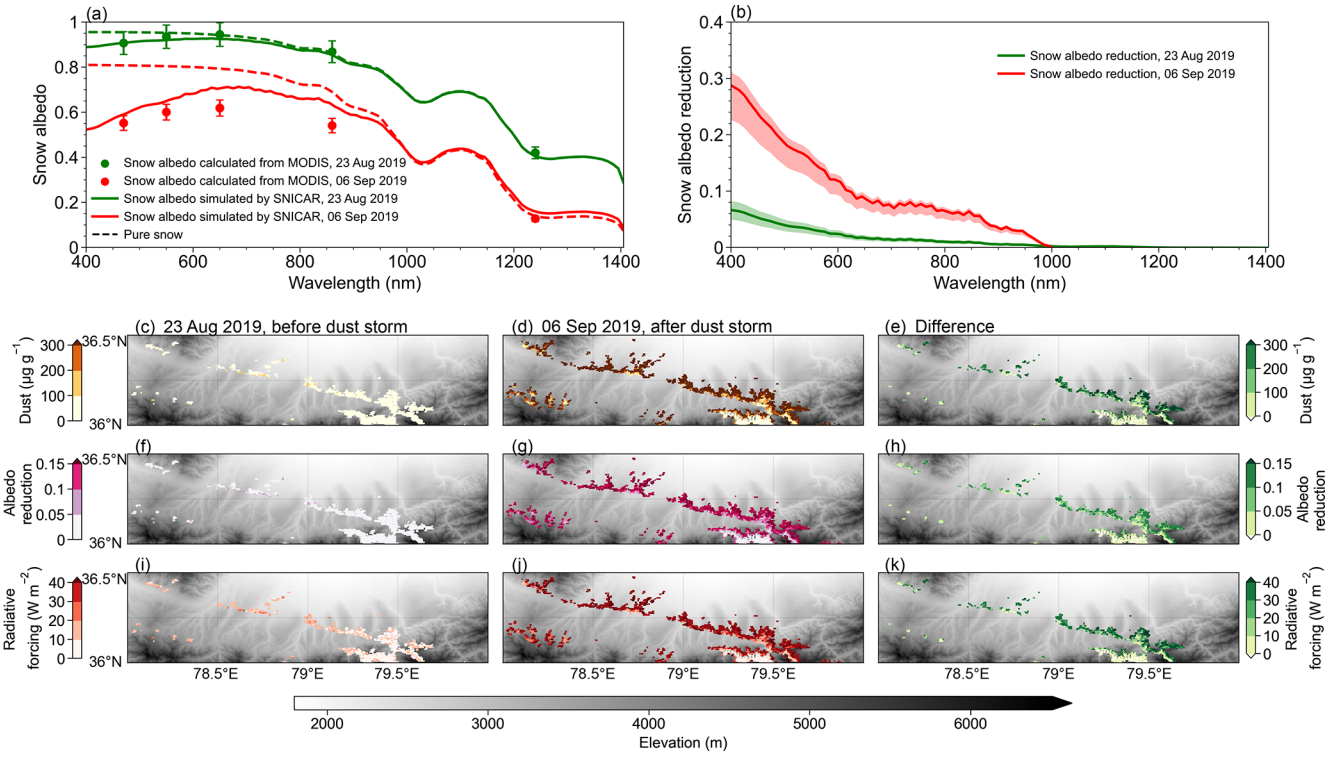

Figure 7. Panel **(a)** shows the averaged SNICAR-simulated spectral snow albedo (solid lines) and MODIS-derived five-band snow albedo (dots) for the region across the Kunlun Mountains impacted by the 26 August to 8 September 2019 severe dust event. Panel **(b)** shows the snow albedo reductions on 23 August 2019 (green) and 6 September 2019 (red). Shadings indicate the retrieval uncertainty. Spatial distributions of the average **(c, d)** dust, **(f, g)** albedo reduction, and **(i, j)** radiative forcing on 23 August and 6 September 2019, respectively. Spatial distributions of the differences in **(e)** dust, **(h)** albedo reduction, and **(k)** radiative forcing between 23 August and 6 September 2019. The background image in **(c)**–**(k)** is a grayscale topographic map of the Kunlun Mountains.

growth (Fig. S9), also contributed to the observed increase in snow albedo reduction (radiative forcing); this trend was similar to that observed across the Kunlun Mountains. Figure S5i–l show the overall uncertainty in snow albedo reduction retrieval in the Qilian Mountains, with the uncertainty bounds averaging 16 % (−21 %) on 1 November and 11 % (−20 %) on 4 November, respectively. Our approach uses satellite remote sensing to obtain a more complete spatiotemporal evolution of the TD dust storm, including its emission, long-range transport, and deposition, across the Qilian Mountains, which offers advantages over previous field measurements (Wei et al., 2017).

3.2 Contributions to the spatial and altitudinal variations in dust-induced snow darkening

We quantified the contributions of the three key factors (dust content, snow properties, and solar zenith) to the spatial variations in snow albedo reduction (Fig. 10) using the method described in Sect. 2.6. The dust content was the dominant contributor to the spatial variations in snow darkening. This is at least partially attributed to the greater spatial differences in dust content compared with those of the other factors, as shown in Figs. 5, 7, and 9. Furthermore, theoretical modeling has indicated that the snow albedo reduction is more sensitive to changes in dust content than to changes in the snow properties and solar zenith angle (Flanner et al., 2021; Usha et al., 2022; Zhao et al., 2022). Laboratory experiments also support these findings (Zhang et al., 2018; Li et al., 2022). The contribution of the dust content also increased as the elevation in each mountain range increased, whereas a decreasing trend was observed for the snow parameters. This is because the dust content exhibits spatial differences across all of the elevations owing to its widespread and heterogeneous depositions. However, the snow depth has a more semi-infinite nature and R_{eff} exhibits greater spatial homogeneity at higher elevations owing to slower snow aging.

Scatter plots of the snow albedo reduction for the elevations across the Tien Shan, Kunlun, and Qilian mountains are shown in Fig. 11. The snow albedo reduction across the Tien Shan decreased with increasing elevation prior to the dust storm. However, the most severe dust deposition occurred within the 4000–4500 m elevation range, resulting in the most significant enhancement of snow albedo reduction in this elevation range. These findings are consistent with those reported for the Himalayas (Sarangi et al., 2020). The

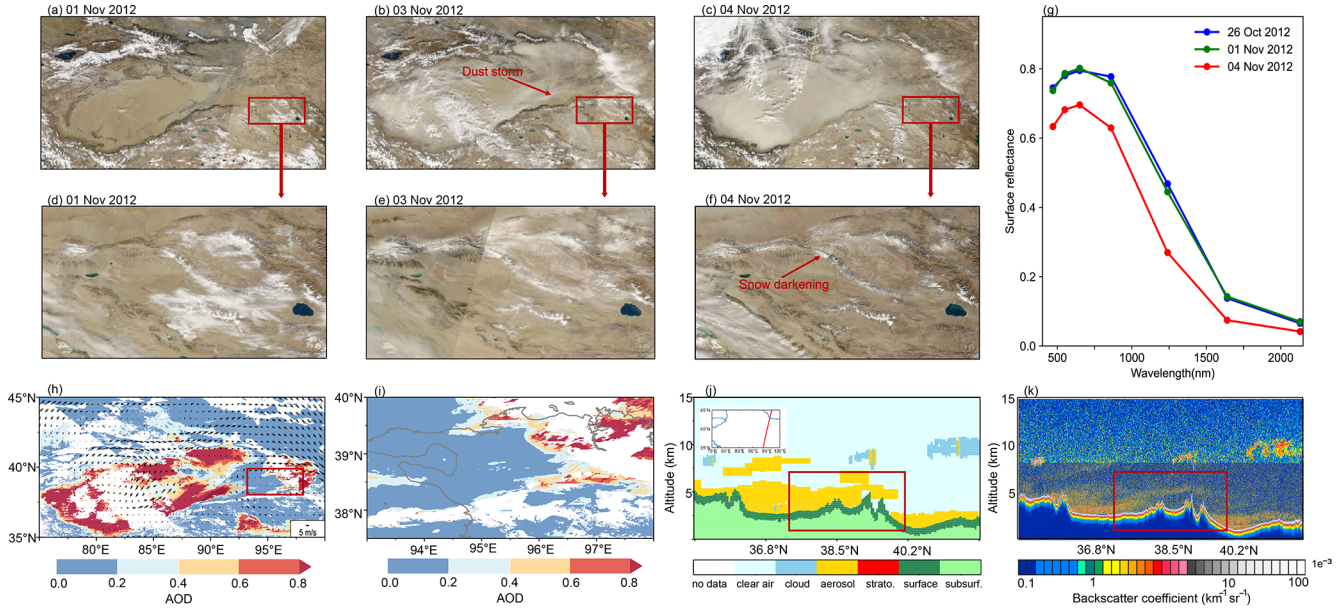

Figure 8. Satellite observations during the 2–4 November 2012 dust storm across the Qilian Mountains. Panels **(a)** and **(d)** are Terra/MODIS satellite true-color images acquired on 1 November 2012, prior to the dust storm. Panels **(b)** and **(e)** are Terra/MODIS satellite images acquired on 3 November 2012, with the dust transport from the TD to the Qilian Mountains indicated by the red arrow in **(b)**. Panels **(c)** and **(f)** are Terra/MODIS satellite images acquired on 4 November 2012, with significant snow darkening observed across the Qilian Mountains after the dust storm. Satellite images **(a)**–**(f)** are from Terra/MODIS (https://worldview.earthdata.nasa.gov, last access: 19 April 2024). Panel **(g)** shows MOD09GA spectral surface reflectance over the snow-covered areas on 26 October 2012 (blue), 1 November 2012 (green), and 4 November 2012 (red). Panel **(h)** is a MODIS AOD image acquired on 3 November 2012, with the ERA5 daily mean wind vector at 700 hPa overlain. Panel **(i)** is a MODIS AOD image across the Qilian Mountains from 3 November 2012. The gray line denotes the 3000 m elevation contour. CALIPSO **(j)** vertical feature mask and **(k)** backscatter coefficient on 3 November 2012.

snow albedo reduction was generally low across the Kunlun Mountains for all of the elevation ranges. However, dust deposition caused the most significant albedo reduction within the 4500–5500 m elevation range, with a dramatic decrease in its influence above 6000 m. These findings correspond to the CALIPSO aerosol vertical profile observations (Fig. 6j and k). The snow albedo reduction across the Qilian Mountains initially increased with elevation up to $\sim$5000 m and then decreased at high elevations prior to the dust storm. However, the most severe dust deposition occurred across the lower elevations, leading to the most significant enhancement of snow albedo reduction across these lower-elevation regions. Our elevation analysis revealed a consistent outcome whereby the dust storms significantly darkened the snowpack up to $>$ 5000 m elevation across the three analyzed mountain ranges.

4 Discussion

The snow darkening effect and its resultant radiative forcing have gained increasing attention in recent decades owing to their significant impacts on regional climate and hydrological systems. However, studies in the Tien Shan, Kunlun, and Qilian mountains have been limited to local-scale observations, despite the significant impact of dust on snow darkening in these regions. Here we provide an overview of previous in situ dust-content measurements in the snowpack across the study region for comparison with our satellite remote-sensing results (see Fig. 12). In the Tien Shan region, Ming et al. (2016), Xu et al. (2016), Li et al. (2021), and X. Zhang et al. (2021) reported a dust content of 19.3–110 $\mu g\,g^{-1}$ in the snowpack across Urumqi Glacier No. 1. Dong et al. (2009) observed an average dust content of 0.97–3.69 $\mu g\,g^{-1}$ in the snowpack across Urumqi Glacier No. 1, Haxilegen Glacier No. 51, and Miaoergou Glacier. Schmale et al. (2017) found a variable dust content of 68.1–125.9 $\mu g\,g^{-1}$ in the snowpack across Suek Zapadniy, No. 354, and Golubin glaciers in the western Tien Shan. In the Kunlun Mountains, Wake et al. (1994) reported a dust content of up to $\sim$8 $\mu g\,g^{-1}$ in the snow/ice across the western Kunlun Mountains. Wu et al. (2010) and Xu et al. (2016) measured dust contents of $\sim$8.68 and 16.24 $\mu g\,g^{-1}$ in the ice core and snowpack across Muztagata Glacier in the northwestern Tibetan Plateau (Wu et al., 2010; Xu et al., 2016), respectively. In the Qilian Mountains, Wu et al. (2010) analyzed ice cores from Dunde Glacier and measured a dust content of $\sim$21 $\mu g\,g^{-1}$. The measured dust contents in the snowpack across Laohugou Glacier ranged from around 3 to 93.2 $\mu g\,g^{-1}$ (Dong et al., 2014; Xu et al., 2016; Zhang et al., 2018; Li et al., 2022).

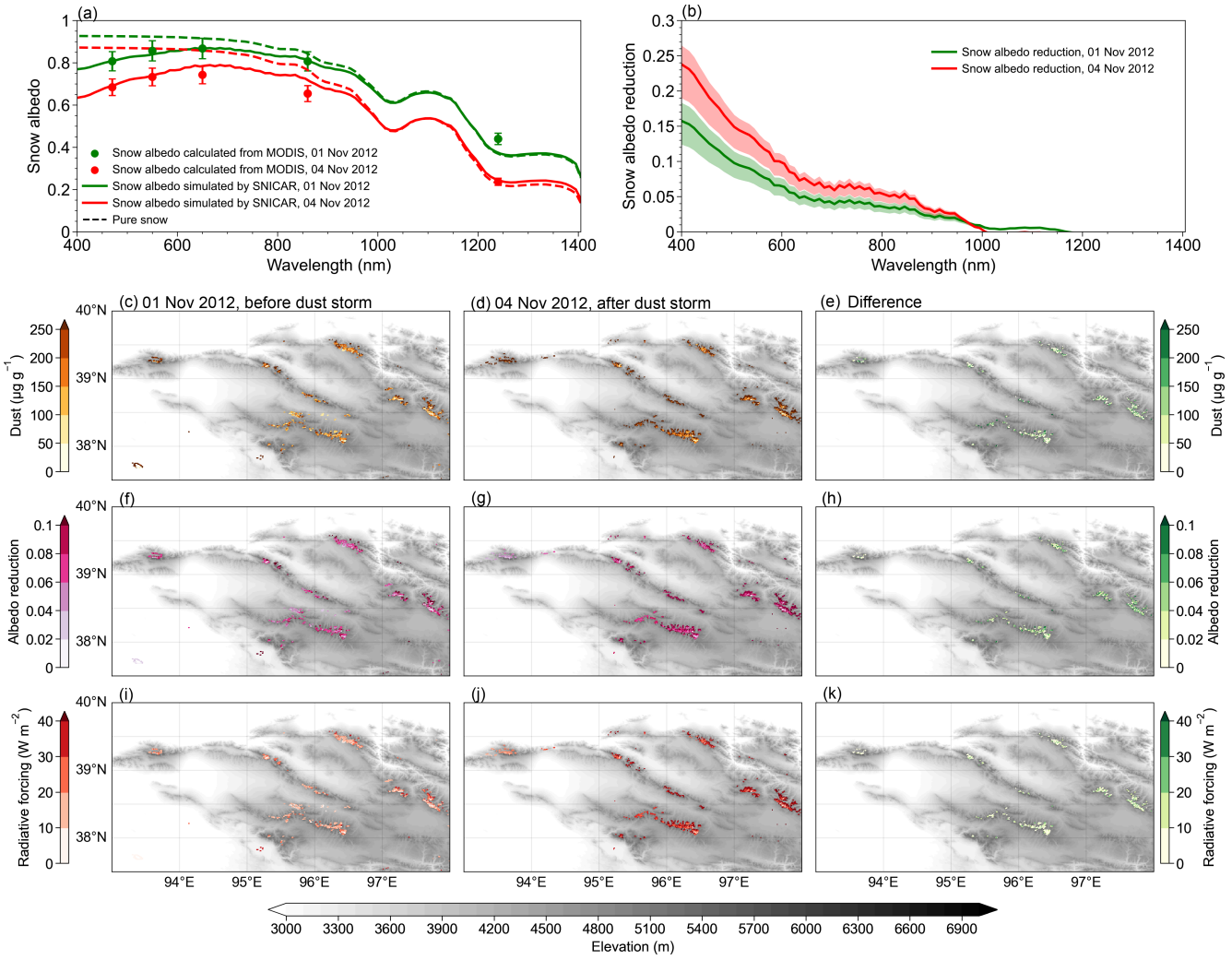

Figure 9. Panel **(a)** shows the averaged SNICAR-simulated spectral snow albedo (solid lines) and MODIS-derived five-band snow albedo (dots) for the region across the Qilian Mountains impacted by the 2–4 November 2012 severe dust event. Panel **(b)** shows the snow albedo reductions on 1 November 2012 (green) and 4 November 2012 (red). Shadings indicate the retrieval uncertainty. Spatial distributions of the average **(c, d)** dust, **(f, g)** albedo reduction, and **(i, j)** radiative forcing on 1 and 4 November 2012, respectively. Spatial distributions of the differences in **(e)** dust, **(h)** albedo reduction, and **(k)** radiative forcing between 1 and 4 November 2012. The background image in **(c)**–**(k)** is a grayscale image of the Qilian Mountains.

Wang et al. (2019) measured a variable dust content of 1.4–1.9 $\mu g\,g^{-1}$ in the fresh snow across Qiyi, Meikuang, and Yuzhufeng glaciers. Overall, previous field studies have reported dust contents of 0.97–125.9, 6.78–16.24, and 1.4–93.2 $\mu g\,g^{-1}$ for the Tien Shan, Kunlun, and Qilian mountains, respectively.

Our satellite-derived approach has yielded much higher dust contents than those obtained via in situ field measurements, with 42–196, 170–360, and 194–360 $\mu g\,g^{-1}$ determined for the Tien Shan, Kunlun, and Qilian mountains, respectively. A key reason for this discrepancy could be that the field measurements usually record the background dust content signal, which includes a gradual natural deposition of dust, whereas our analysis specifically focused on significant snow darkening events due to severe dust storms, which further highlights the advantage of employing remote-sensing techniques to observe extreme snow darkening phenomena (Li et al., 2020). We do note that satellite-derived approaches possess their own uncertainties, which arise from the data resolution and accuracy, algorithm assumptions, as well as atmospheric and underlying surface interferences (Cui et al., 2021). Nevertheless, this satellite-derived approach remains a valuable tool for effectively and rapidly studying extreme events, which cannot be captured by field measurements or climate model simulations, particularly as these extreme events will become increasingly important for climate and hydrological systems as the global climate continues to warm (Clow et al., 2016; Dumont et al., 2020).

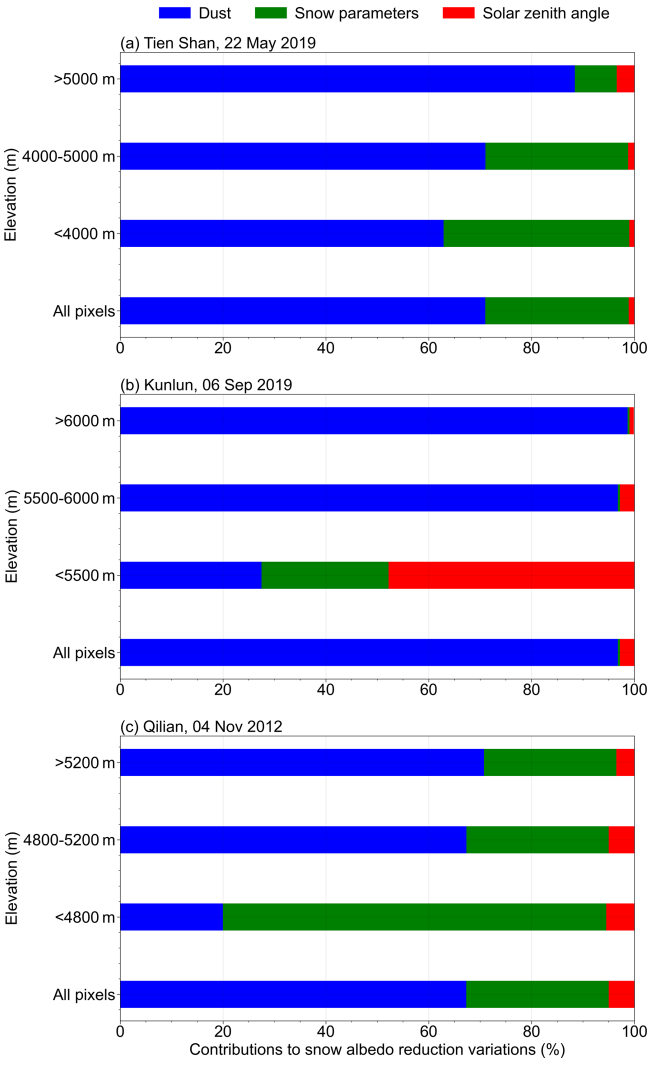

Figure 10. Contributions of the spatial variations in dust content (blue), snow parameters (green), and solar zenith angle (red) to the snow albedo reduction at different elevations across the **(a)** Tien Shan, **(b)** Kunlun, and **(c)** Qilian mountains.

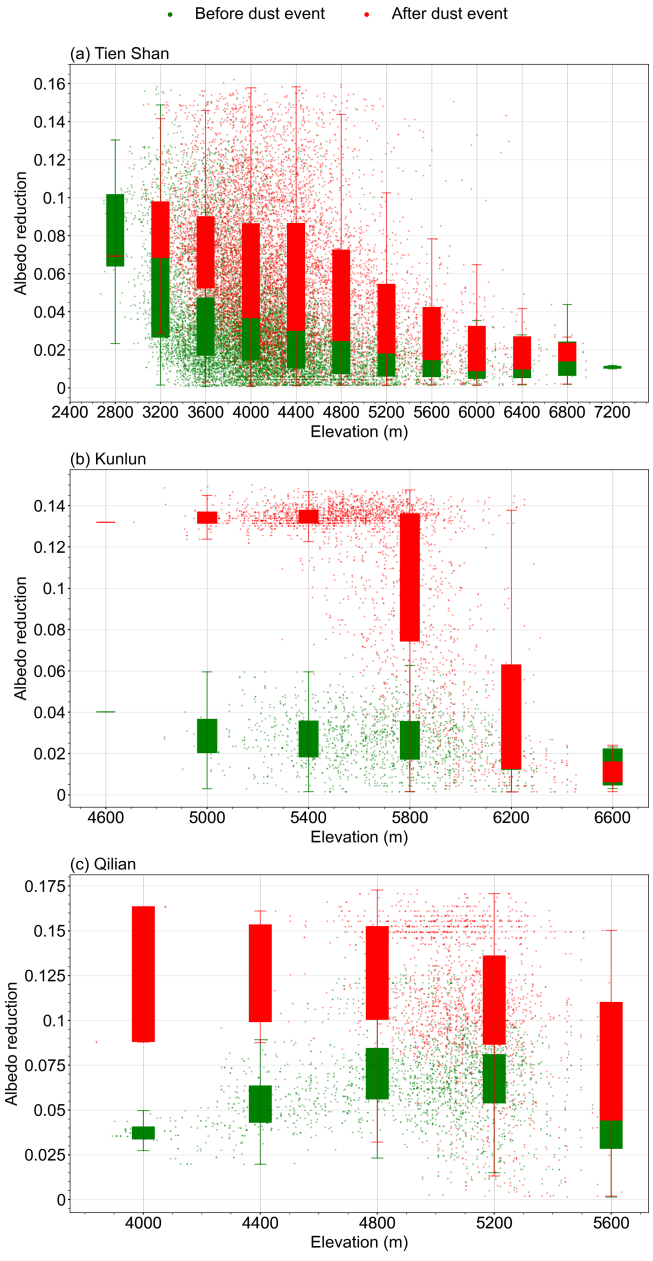

Figure 11. Scatter plots of the snow albedo reductions for the analyzed elevation ranges across the **(a)** Tien Shan, **(b)** Kunlun, and **(c)** Qilian mountains. Each box plot shows the statistical results for a 400 m elevation interval.

Given the significant snow darkening effect highlighted in this study and recent observations of decreasing snow cover across the Tien Shan, Kunlun, and Qilian mountains (She et al., 2015; Li et al., 2020; Zhu et al., 2022), it is crucial to evaluate the impact of snow darkening on regional hydrological cycles and local freshwater supplies. However, snow aging and melting mechanisms are complex and therefore require complementary observations, because remote sensing alone cannot distinguish the influences of augmented shortwave radiation owing to dust and increased air temperatures on snow aging and melting (Gautam et al., 2013). Additional research that integrates model simulations and satellite observations is necessary to differentiate the roles of snow darkening and global warming in enhancing snow aging and melting, and the resultant changes in glacier runoff in the future.

5 Conclusions

Our study focused on the impact of the annual vast dust emissions from the Taklamakan Desert on the surrounding high mountain snowpack. Using a combination of MODIS satellite data analysis and SNICAR model simulations, we aimed to reveal significant snow darkening events and quantify the resulting snow albedo reduction and radiative forcing caused by severe dust storms. Our analysis of the satel-

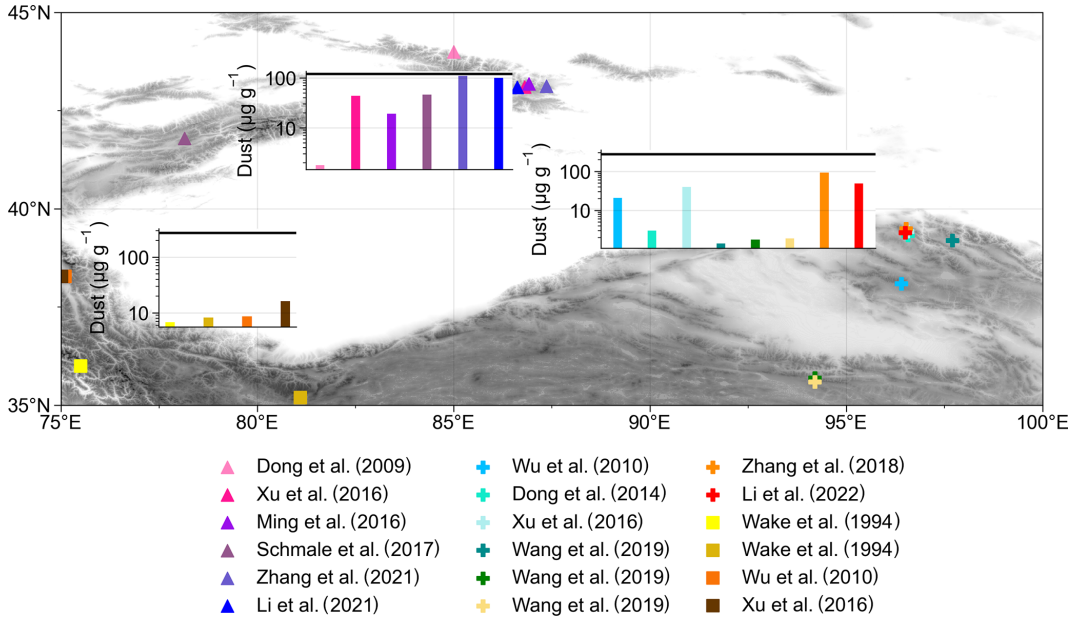

Figure 12. Comparisons of the satellite-derived dust contents (black lines) in snow from this study and observed values from previous studies (colored symbols and bars).

lite data revealed significant snow darkening over the 3000–6000 m elevation range across the Tien Shan and Kunlun mountains. This phenomenon was attributed to the high uplift of dust owing to the local topography and atmospheric circulation. The impacted area, spanning the track of the dust storm, encompassed almost all of the snow-covered areas across the Tien Shan ($> 2100\,km^2$) and Kunlun ($> 600\,km^2$) mountains, including the summits. The dust content in the snowpack increased to 42–192 and 170–360 $\mu g\,g^{-1}$, resulting in significant increases in snow albedo reduction (radiative forcing) of 0.028–0.079 (11–31.5 $W\,m^{-2}$) and 0.088–0.136 (31–49 $W\,m^{-2}$) across the Tien Shan and Kunlun mountains, respectively. Additionally, the dust storms accelerated snow aging, as indicated by the growth of R_{eff}. Furthermore, the dust plumes from the Taklamakan Desert traveled eastward, depositing dust across much of the snow-covered area ($> 630\,km^2$) in the Qilian Mountains, where the dust content significantly increased to 194–360 $\mu g\,g^{-1}$, causing a considerable increase in snow albedo reduction (radiative forcing) of 0.092–0.153 (22–38 $W\,m^{-2}$). The spatial distribution of the snow darkening effect varied across all three mountain ranges due to the uneven deposition of dust, with the most significant snow darkening observed in the high-elevation range of 4000–5500 m. Moreover, by comparing our satellite-derived results with previous field measurements, we found that severe dust storms, occurring over short periods, have a more profound effect on snow darkening compared with the relatively slow deposition of dust in the absence of dust storms. These severe snow darkening events were not limited to the three typical cases but instead occurred widely (Figs. S13–S21). This highlights the importance of satellite-derived analyses in capturing extreme dust deposition events that may be challenging to detect through field measurements and climate model simulations. Our findings underscore the significance of understanding the impact of dust deposition on snow albedo and radiative forcing for accurate assessment of the environmental effects of these extreme events.

Data availability. All datasets and codes used to produce this study can be obtained by contacting Wei Pu (puwei@lzu.edu.cn).

Supplement. The supplement related to this article is available online at: https://doi.org/10.5194/acp-24-5199-2024-supplement.

Author contributions. WP and XW designed the study and developed the overarching research goals and aims. YX carried the study out and wrote the first draft with contributions from all co-authors. YX processed the data with the assistance of YC, SY, TS, XC, XN, DW, JC, and YZ. WP and XW assumed oversight and leadership responsibility for the research activity planning and execution. All authors contributed to the improvement of results and revised the final paper.

Competing interests. The contact author has declared that none of the authors has any competing interests.

Acknowledgements. The Lanzhou University group acknowledges support from the National Science Fund for Distinguished Young Scholars, the State Key Laboratory of Cryosphere Science Open Fund, and the National Natural Science Foundation of China. We appreciate Boyuan Zhang's assistance with the code improvements. We thank Lanzhou City's scientific research funding subsidy to Lanzhou University and the Supercomputing Center of Lanzhou University for providing the computing services. We also appreciate the insightful comments provided by the editor and the three reviewers.

Financial support. This research was supported by the National Science Fund for Distinguished Young Scholars (grant no. 42025102), the State Key Laboratory of Cryosphere Science Open Fund (grant no. SKLCS-OP-2021-05) and the National Natural Science Foundation of China (grant nos. 42375068 and 42075061), and the Natural Science Foundation of Gansu province, China (grant no. 21ZDKA0017).

Review statement. This paper was edited by Pedro Jimenez-Guerrero and reviewed by three anonymous referees.

References

Arun, B. S., Aswini, A. R., Gogoi, M. M., Hegde, P., Kumar Kompalli, S., Sharma, P., and Suresh Babu, S.: Physico-chemical and optical properties of aerosols at a background site (∼ 4 km a.s.l.) in the western Himalayas, Atmos. Environ., 218, 117017, https://doi.org/10.1016/j.atmosenv.2019.117017, 2019.

Arun, B. S., Gogoi, M. M., Borgohain, A., Hegde, P., Kundu, S. S., and Babu, S. S.: Role of sulphate and carbonaceous aerosols on the radiative effects of aerosols over a remote high-altitude site Lachung in the Eastern Himalayas, Atmos. Res., 263, 105799, https://doi.org/10.1016/j.atmosres.2021.105799, 2021a.

Arun, B. S., Gogoi, M. M., Hegde, P., Borgohain, A., Boreddy, S. K. R., Kundu, S. S., and Babu, S. S.: Carbonaceous Aerosols over Lachung in the Eastern Himalayas: Primary Sources and Secondary Formation of Organic Aerosols in a Remote High-Altitude Environment, ACS Earth Space Chem., 5, 2493–2506, https://doi.org/10.1021/acsearthspacechem.1c00190, 2021b.

Bair, E. H., Stillinger, T., and Dozier, J.: Snow property inversion from remote sensing (SPIReS): A generalized multispectral unmixing approach with examples from MODIS and Landsat 8 OLI, IEEE T. Geosci. Remote, 59, 7270–7284, https://doi.org/10.1109/tgrs.2020.3040328, 2020.

Baladima, F., Thomas, J. L., Voisin, D., Dumont, M., Junquas, C., Kumar, R., Lavaysse, C., Marelle, L., Parrington, M., and Flemming, J.: Modeling an extreme dust deposition event to the French Alpine seasonal snowpack in April 2018: Meteorological context and predictions of dust deposition, J. Geophys. Res.-Atmos., 127, e2021JD035745, https://doi.org/10.1029/2021jd035745, 2022.

Bormann, K. J., Brown, R. D., Derksen, C., and Painter, T. H.: Estimating snow-cover trends from space, Nat. Clim. Change, 11, 924–928, https://doi.org/10.1038/s41558-018-0318-3, 2018.

Chaubey, J. P., Moorthy, K. K., Babu, S. S., Nair, V. S., and Tiwari, A.: Black carbon aerosols over coastal Antarctica and its scavenging by snow during the Southern Hemispheric summer, J. Geophys. Res.-Atmos., 115, D10210, https://doi.org/10.1029/2009jd013381, 2010.

Chen, B., Song, Z., Huang, J., Zhang, P., Hu, X., Zhang, X., Guan, X., Ge, J., and Zhou, X.: Estimation of atmospheric PM_{10} Concentration in China using an interpretable deep learning model and top-of-the-atmosphere reflectance data from China's new generation geostationary meteorological satellite, FY-4A, J. Geophys. Res.-Atmos., 127, e2021JD036393, https://doi.org/10.1029/2021jd036393, 2022.

Chen, S., Huang, J., Zhao, C., Qian, Y., Leung, L. R., and Yang, B.: Modeling the transport and radiative forcing of Taklimakan dust over the Tibetan Plateau: A case study in the summer of 2006, J. Geophys. Res.-Atmos., 118, 797–812, https://doi.org/10.1002/jgrd.50122, 2013.

Chen, S., Huang, J., Kang, L., Wang, H., Ma, X., He, Y., Yuan, T., Yang, B., Huang, Z., and Zhang, G.: Emission, transport, and radiative effects of mineral dust from the Taklimakan and Gobi deserts: comparison of measurements and model results, Atmos. Chem. Phys., 17, 2401–2421, https://doi.org/10.5194/acp-17-2401-2017, 2017a.

Chen, S., Huang, J., Li, J., Jia, R., Jiang, N., Kang, L., Ma, X., and Xie, T.: Comparison of dust emissions, transport, and deposition between the Taklimakan Desert and Gobi Desert from 2007 to 2011, Sci. China Earth Sci., 60, 1338–1355, https://doi.org/10.1007/s11430-016-9051-0, 2017b.

Chen, W., Wang, X., Cui, J., Cao, X., Pu, W., Zheng, X., Ran, H., and Ding, J.: Radiative forcing of black carbon in seasonal snow of wintertime based on remote sensing over Xinjiang, China, Atmos. Environ., 247, 118204, https://doi.org/10.1016/j.atmosenv.2021.118204, 2021.

Clow, D. W., Williams, M. W., and Schuster, P. F.: Increasing aeolian dust deposition to snowpacks in the Rocky Mountains inferred from snowpack, wet deposition, and aerosol chemistry, Atmos. Environ., 146, 183–194, https://doi.org/10.1016/j.atmosenv.2016.06.076, 2016.

Cohen, J. and Rind, D.: The Effect of Snow Cover on the Climate, J. Climate, 4, 689–706, https://doi.org/10.1175/1520-0442(1991)004<0689:TEOSCO>2.0.CO;2, 1991.

Copernicus Climate Change Service: ERA5: Fifth generation of ECMWF atmospheric reanalysis of the global climate, Copernicus Climate Change Service Climate Data Store (CDS), https://climate.copernicus.eu/era5-new-dataset-monthly-climate-bulletin (last access: 25 April 2024), 2017.

Cordero, R., Sepúlveda, E., Feron, S., Damiani, A., Fernandoy, F., Neshyba, S., Rowe, P. M., Asencio, V., Carrasco, J., Alfonso, J. A., Llanillo, P., Wachter, P., Seckmeyer, G., Stepanova, M., Carrera, J. M., Jorquera, J., Wang, C., Malhotra, A., Dana, J., Khan, A. L., and Casassa, G.: Black carbon footprint of hu-

man presence in Antarctica, Nat. Commun., 13, 2041–1723, https://doi.org/10.1038/s41467-022-28560-w, 2022.

Cui, J., Shi, T., Zhou, Y., Wu, D., Wang, X., and Pu, W.: Satellite-based radiative forcing by light-absorbing particles in snow across the Northern Hemisphere, Atmos. Chem. Phys., 21, 269–288, https://doi.org/10.5194/acp-21-269-2021, 2021.

Cui, J., Niu, X., Chen, Y., Xing, Y., Yan, S., Zhao, J., Chen, L., Xu, S., Wu, D., Shi, T., Wang, X., and Pu, W.: The Spatio-Temporal Variability in the Radiative Forcing of Light-Absorbing Particles in Snow of 2003–2018 over the Northern Hemisphere from MODIS, Remote Sensing, 15, 636, https://doi.org/10.3390/rs15030636, 2023.

Dang, C., Warren, S. G., Fu, Q., Doherty, S. J., Sturm, M., and Su, J.: Measurements of light-absorbing particles in snow across the Arctic, North America, and China: Effects on surface albedo, J. Geophys. Res.-Atmos., 122, 10149–10168, https://doi.org/10.1002/2017jd027070, 2017.

Di Mauro, B., Fava, F., Ferrero, L., Garzonio, R., Baccolo, G., Delmonte, B., and Colombo, R.: Mineral dust impact on snow radiative properties in the European Alps combining ground, UAV, and satellite observations, J. Geophys. Res.-Atmos., 120, 6080–6097, https://doi.org/10.1002/2015jd023287, 2015.

Dong, Q., Huang, Z., Li, W., Li, Z., Song, X., Liu, W., Wang, T., Bi, J., and Shi, J.: Polarization lidar measurements of dust optical properties at the junction of the Taklimakan Desert–Tibetan Plateau, Remote Sens.-Basel, 14, 558, https://doi.org/10.3390/rs14030558, 2022.

Dong, Z., Li, Z., Wang, F., and Zhang, M.: Characteristics of atmospheric dust deposition in snow on the glaciers of the eastern Tien Shan, China, J. Glaciol., 55, 797–804, https://doi.org/10.3189/002214309790152393, 2009.

Dong, Z., Qin, D., Chen, J., Qin, X., Ren, J., Cui, X., Du, Z., and Kang, S.: Physicochemical impacts of dust particles on alpine glacier meltwater at the Laohugou Glacier basin in western Qilian Mountains, China, Sci. Total Environ., 493, 930–942, https://doi.org/10.1016/j.scitotenv.2014.06.025, 2014.

Dong, Z., Brahney, J., Kang, S., Elser, J., Wei, T., Jiao, X., and Shao, Y.: Aeolian dust transport, cycle and influences in high-elevation cryosphere of the Tibetan Plateau region: New evidences from alpine snow and ice, Earth-Sci. Rev., 211, 103408, https://doi.org/10.1016/j.earscirev.2020.103408, 2020.

Dumont, M., Brun, E., Picard, G., Michou, M., Libois, Q., Petit, J. R., Geyer, M., Morin, S., and Josse, B.: Contribution of light-absorbing impurities in snow to Greenland's darkening since 2009, Nat. Geosci., 7, 509–512, https://doi.org/10.1038/ngeo2180, 2014.

Dumont, M., Tuzet, F., Gascoin, S., Picard, G., Kutuzov, S., Lafaysse, M., Cluzet, B., Nheili, R., and Painter, T. H.: Accelerated snow melt in the Russian Caucasus Mountains after the Saharan dust outbreak in March 2018, J. Geophys. Res.-Earth, 125, e2020JF005641, https://doi.org/10.1029/2020jf005641, 2020.

Flanner, M. G., Zender, C. S., Randerson, J. T., and Rasch, P. J.: Present-day climate forcing and response from black carbon in snow, J. Geophys. Res., 112, D11202, https://doi.org/10.1029/2006jd008003, 2007.

Flanner, M. G., Zender, C. S., Hess, P. G., Mahowald, N. M., Painter, T. H., Ramanathan, V., and Rasch, P. J.: Springtime warming and reduced snow cover from carbonaceous particles, Atmos. Chem. Phys., 9, 2481–2497, https://doi.org/10.5194/acp-9-2481-2009, 2009.

Flanner, M. G., Arnheim, J. B., Cook, J. M., Dang, C., He, C., Huang, X., Singh, D., Skiles, S. M., Whicker, C. A., and Zender, C. S.: SNICAR-ADv3: a community tool for modeling spectral snow albedo, Geosci. Model Dev., 14, 7673–7704, https://doi.org/10.5194/gmd-14-7673-2021, 2021.

Gautam, R., Hsu, N. C., Lau, W. K. M., and Yasunari, T. J.: Satellite observations of desert dust-induced Himalayan snow darkening, Geophys. Res. Lett., 40, 988–993, https://doi.org/10.1002/grl.50226, 2013.

Ge, J. M., Huang, J. P., Xu, C. P., Qi, Y. L., and Liu, H. Y.: Characteristics of Taklimakan dust emission and distribution: A satellite and reanalysis field perspective, J. Geophys. Res.-Atmos., 119, 11772–711783, https://doi.org/10.1002/2014jd022280, 2014.

Gogoi, M. M., Babu, S. S., Pandey, S. K., Nair, V. S., Vaishya, A., Girach, I. A., and Koushik, N.: Scavenging ratio of black carbon in the Arctic and the Antarctic, Polar Sci., 16, 10–22, https://doi.org/10.1016/j.polar.2018.03.002, 2018.

Gogoi, M. M., Babu, S. S., Arun, B. S., Moorthy, K. K., Ajay, A., Ajay, P., Suryavanshi, A., Borgohain, A., Guha, A., Shaikh, A., Pathak, B., Gharai, B., Ramasamy, B., Balakrishnaiah, G., Menon, H. B., Kuniyal, J. C., Krishnan, J., Gopal, K. R., Maheswari, M., Naja, M., Kaur, P., Bhuyan, P. K., Gupta, P., Singh, P., Srivastava, P., Singh, R. S., Kumar, R., Rastogi, S., Kundu, S. S., Kompalli, S. K., Panda, S., Rao, T. C., Das, T., and Kant, Y.: Response of ambient BC concentration across the Indian region to the nation-wide lockdown: results from the ARFINET measurements of ISRO-GBP, Curr. Sci. India, 120, 341–351, 2021a.

Gogoi, M. M., Pandey, S. K., Arun, B. S., Nair, V. S., Thakur, R. C., Chaubey, J. P., Tiwari, A., Manoj, M. R., Kompalli, S. K., Vaishya, A., Prijith, S. S., Hegde, P., and Babu, S. S.: Long-term changes in aerosol radiative properties over Ny-Ålesund: Results from Indian scientific expeditions to the Arctic, Polar Sci., 30, 100700, https://doi.org/10.1016/j.polar.2021.100700, 2021b.

Gui, K., Yao, W., Che, H., An, L., Zheng, Y., Li, L., Zhao, H., Zhang, L., Zhong, J., Wang, Y., and Zhang, X.: Record-breaking dust loading during two mega dust storm events over northern China in March 2021: aerosol optical and radiative properties and meteorological drivers, Atmos. Chem. Phys., 22, 7905–7932, https://doi.org/10.5194/acp-22-7905-2022, 2022.

Hadley, O. L. and Kirchstetter, T. W.: Black-carbon reduction of snow albedo, Nat. Clim. Change, 2, 437–440, https://doi.org/10.1038/nclimate1433, 2012.

Han, Y., Wang, T., Tang, J., Wang, C., Jian, B., Huang, Z., and Huang, J.: New insights into the Asian dust cycle derived from CALIPSO lidar measurements, Remote Sens. Environ., 272, 112906. https://doi.org/10.1016/j.rse.2022.112906, 2022.

He, C., Takano, Y., Liou, K.-N., Yang, P., Li, Q., and Chen, F.: Impact of snow grain shape and black carbon–snow internal mixing on snow optical properties: Parameterizations for climate models, J. Climate, 30, 10019–10036, https://doi.org/10.1175/jcli-d-17-0300.1, 2017.

He, C., Liou, K. N., Takano, Y., Yang, P., Qi, L., and Chen, F.: Impact of grain shape and multiple black carbon internal mixing on snow albedo: Parameterization and radiative effect analysis, J. Geophys. Res.-Atmos., 123, 1253–1268, https://doi.org/10.1002/2017jd027752, 2018.

Huang, H., Qian, Y., He, C., Bair, E. H., and Rittger, K.: Snow albedo feedbacks enhance snow impurity-induced radiative forcing in the Sierra Nevada, Geophys. Res. Lett., 49, e2022GL098102, https://doi.org/10.1029/2022GL098102, 2022.

Huang, J., Minnis, P., Yi, Y., Tang, Q., Wang, X., Hu, Y., Liu, Z., Ayers, K., Trepte, C., and Winker, D.: Summer dust aerosols detected from CALIPSO over the Tibetan Plateau, Geophys. Res. Lett., 34, L18805, https://doi.org/10.1029/2007gl029938, 2007.

Huang, J., Minnis, P., Chen, B., Huang, Z., Liu, Z., Zhao, Q., Yi, Y., and Ayers, J. K.: Long-range transport and vertical structure of Asian dust from CALIPSO and surface measurements during PACDEX, J. Geophys. Res., 113, D23212, https://doi.org/10.1029/2008jd010620, 2008.

Huang, J., Wang, T., Wang, W., Li, Z., and Yan, H.: Climate effects of dust aerosols over East Asian arid and semiarid regions, J. Geophys. Res.-Atmos., 119, 11398–11416, https://doi.org/10.1002/2014jd021796, 2014.

Immerzeel, W. W. and Bierkens, M. F. P.: Asia's water balance, Nat. Geosci., 5, 841–842, https://doi.org/10.1038/ngeo1643, 2012.

Jia, R., Liu, Y., Chen, B., Zhang, Z., and Huang, J.: Source and transportation of summer dust over the Tibetan Plateau, Atmos. Environ., 123, 210–219, https://doi.org/10.1016/j.atmosenv.2015.10.038, 2015.

Kang, L., Huang, J., Chen, S., and Wang, X.: Long-term trends of dust events over Tibetan Plateau during 1961–2010, Atmos. Environ., 125, 188–198, https://doi.org/10.1016/j.atmosenv.2015.10.085, 2016.

Kraaijenbrink, P. D. A., Bierkens, M. F. P., Lutz, A. F., and Immerzeel, W. W.: Impact of a global temperature rise of 1.5 degrees Celsius on Asia's glaciers, Nature, 549, 257–260, https://doi.org/10.1038/nature23878, 2017.

Kraaijenbrink, P. D. A., Stigter, E. E., Yao, T., and Immerzeel, W. W.: Climate change decisive for Asia's snow meltwater supply, Nat. Clim. Change, 11, 591–597, https://doi.org/10.1038/s41558-021-01074-x, 2021.

Li, Y., Chen, Y., and Li, Z.: Climate and topographic controls on snow phenology dynamics in the Tienshan Mountains, Central Asia, Atmos. Res., 236, 104813, https://doi.org/10.1016/j.atmosres.2019.104813, 2020.

Li, Y., Kang, S., Zhang, X., Chen, J., Schmale, J., Li, X., Zhang, Y., Niu, H., Li, Z., Qin, X., He, X., Yang, W., Zhang, G., Wang, S., Shao, L., and Tian, L.: Black carbon and dust in the Third Pole glaciers: Revaluated concentrations, mass absorption cross-sections and contributions to glacier ablation, Sci. Total Environ., 789, 147746, https://doi.org/10.1016/j.scitotenv.2021.147746, 2021.

Li, Y., Kang, S., Zhang, X., Li, C., Chen, J., Qin, X., Shao, L., and Tian, L.: Dust dominates the summer melting of glacier ablation zones on the northeastern Tibetan Plateau, Sci. Total Environ., 856, 159214, https://doi.org/10.1016/j.scitotenv.2022.159214, 2022.

Liang, P., Chen, B., Yang, X., Liu, Q., Li, A., Mackenzie, L., and Zhang, D.: Revealing the dust transport processes of the 2021 mega dust storm event in northern China, Sci. Bull., 67, 21–24, https://doi.org/10.1016/j.scib.2021.08.014, 2021.

Meng, L., Yang, X., Zhao, T., He, Q., Lu, H., Mamtimin, A., Huo, W., Yang, F., and Liu, C.: Modeling study on three-dimensional distribution of dust aerosols during a dust storm over the Tarim Basin, Northwest China, Atmos. Res., 218, 285–295, https://doi.org/10.1016/j.atmosres.2018.12.006, 2018.

Ming, J., Xiao, C. D., Wang, F. T., Li, Z. Q., and Li, Y. M.: Grey Tienshan Urumqi Glacier No.1 and light-absorbing impurities, Environ. Sci. Pollut. R., 23, 9549–9558, https://doi.org/10.1007/s11356-016-6182-7, 2016.

Mishra, S. K., Hayse, J., Veselka, T., Yan, E., Kayastha, R. B., LaGory, K., McDonald, K., and Steiner, N.: An integrated assessment approach for estimating the economic impacts of climate change on River systems: An application to hydropower and fisheries in a Himalayan River, Trishuli, Environ. Sci. Policy, 87, 102–111, https://doi.org/10.1016/j.envsci.2018.05.006, 2018.

Mishra, S. K., Rupper, S., Kapnick, S., Casey, K., Chan, H. G., Ciraci, E., Haritashya, U., Hayse, J., Kargel, J. S., Kayastha, R. B., Krakauer, N. Y., Kumar, S. V., Lammers, R. B., Maggioni, V., Margulis, S. A., Olson, M., Osmanoglu, B., Qian, Y., McLarty, S., Rittger, K., Rounce, D. R., Shean, D., Velicogna, I., Veselka, T. D., and Arendt, A.: Grand challenges of hydrologic modeling for food-energy-water nexus security in High Mountain Asia, Frontiers in Water, 3, 728156, https://doi.org/10.3389/frwa.2021.728156, 2021.

Negi, H. S. and Kokhanovsky, A.: Retrieval of snow grain size and albedo of western Himalayan snow cover using satellite data, The Cryosphere, 5, 831–847, https://doi.org/10.5194/tc-5-831-2011, 2011.

Notarnicola, C.: Hotspots of snow cover changes in global mountain regions over 2000–2018, Remote Sens. Environ., 243, 111781, https://doi.org/10.1016/j.rse.2020.111781, 2020.

Niu, X., Pu, W., Fu, P., Chen, Y., Xing, Y., Wu, D., Chen, Z., Shi, T., Zhou, Y., Wen, H., and Wang, X.: Fluorescence characteristics, absorption properties, and radiative effects of water-soluble organic carbon in seasonal snow across northeastern China, Atmos. Chem. Phys., 22, 14075–14094, https://doi.org/10.5194/acp-22-14075-2022, 2022.

Okada, K. and Kai, K.: Atmospheric mineral particles collected at Qira in the Taklamakan Desert, China, Atmos. Environ., 38, 6927–6935, https://doi.org/10.1016/j.atmosenv.2004.03.078, 2004.

Orsolini, Y., Wegmann, M., Dutra, E., Liu, B., Balsamo, G., Yang, K., de Rosnay, P., Zhu, C., Wang, W., Senan, R., and Arduini, G.: Evaluation of snow depth and snow cover over the Tibetan Plateau in global reanalyses using in situ and satellite remote sensing observations, The Cryosphere, 13, 2221–2239, https://doi.org/10.5194/tc-13-2221-2019, 2019.

Painter, T. H., Rittger, K., McKenzie, C., Slaughter, P., Davis, R. E., and Dozier, J.: Retrieval of subpixel snow covered area, grain size, and albedo from MODIS, Remote Sens. Environ., 113, 868–879, https://doi.org/10.1016/j.rse.2009.01.001, 2009.

Painter, T. H., Bryant, A. C., and Skiles, S. M.: Radiative forcing by light absorbing impurities in snow from MODIS surface reflectance data, Geophys. Res. Lett., 39, L17502, https://doi.org/10.1029/2012gl052457, 2012.

Painter, T. H., Skiles, S. M., Deems, J. S., Brandt, W. T., and Dozier, J.: Variation in rising limb of colorado river snowmelt runoff hydrograph controlled by dust radiative forcing in snow, Geophys. Res. Lett., 45, 797–808, https://doi.org/10.1002/2017gl075826, 2017.

Patterson, E. M.: Optical properties of the crustal aerosol: Relation to chemical and physical characteristics, J. Geophys. Res.-Atmos., 86, 3236–3246, https://doi.org/10.1029/JC086iC04p03236, 1981.

Pu, W., Wang, X., Wei, H., Zhou, Y., Shi, J., Hu, Z., Jin, H., and Chen, Q.: Properties of black carbon and other insoluble light-absorbing particles in seasonal snow of northwestern China, The Cryosphere, 11, 1213–1233, https://doi.org/10.5194/tc-11-1213-2017, 2017.

Pu, W., Cui, J., Shi, T., Zhang, X., He, C., and Wang, X.: The remote sensing of radiative forcing by light-absorbing particles (LAPs) in seasonal snow over northeastern China, Atmos. Chem. Phys., 19, 9949–9968, https://doi.org/10.5194/acp-19-9949-2019, 2019.

Pu, W., Cui, J., Wu, D., Shi, T., Chen, Y., Xing, Y., Zhou, Y., and Wang, X.: Unprecedented snow darkening and melting in New Zealand due to 2019–2020 Australian wildfires, Fundamental Research, 1, 224–231, https://doi.org/10.1016/j.fmre.2021.04.001, 2021.

Pulliainen, J., Luojus, K., Derksen, C., Mudryk, L., Lemmetyinen, J., Salminen, M., Ikonen, J., Takala, M., Cohen, J., Smolander, T., and Norberg, J.: Patterns and trends of Northern Hemisphere snow mass from 1980 to 2018, Nature, 581, 294–298, https://doi.org/10.1038/s41586-020-2258-0, 2020.

Qian, Y., Yasunari, T. J., Doherty, S. J., Flanner, M. G., Lau, W. K. M., Ming, J., Wang, H., Wang, M., Warren, S. G., and Zhang, R.: Light-absorbing particles in snow and ice: Measurement and modeling of climatic and hydrological impact, Adv. Atmos. Sci., 32, 64–91, https://doi.org/10.1007/s00376-014-0010-0, 2015.

Qiu, X., Zeng, Y., and Miao, Q.: Sand-dust storms in China: temporal-spatial distribution and tracks of source lands, J. Geogr. Sci., 11, 253–260, https://doi.org/10.1007/BF02892308, 2001.

Réveillet, M., Dumont, M., Gascoin, S., Lafaysse, M., Nabat, P., Ribes, A., Nheili, R., Tuzet, F., Menegoz, M., Morin, S., Picard, G., and Ginoux, P.: Black carbon and dust alter the response of mountain snow cover under climate change, Nat. Commun., 13, 5279, https://doi.org/10.1038/s41467-022-32501-y, 2022.

Ricchiazzi, P., Yang, S. R., Gautier, C., and Sowle, D.: SBDART: A research and teaching software tool for plane-parallell radiative transfer in the Earth's atmosphere, B. Am. Meteorol. Soc., 79, 2101–2114, https://doi.org/10.1175/1520-0477(1998)079<2101:SARATS>2.0.CO;2, 1998.

Rittger, K., Painter, T. H., and Dozier, J.: Assessment of methods for mapping snow cover from MODIS, Adv. Water Resour., 51, 367–380, https://doi.org/10.1016/j.advwatres.2012.03.002, 2013.

Roychoudhury, C., He, C., Kumar, R., McKinnon, J. M., and Arellano, A. F.: On the relevance of aerosols to snow cover variability over High Mountain Asia, Geophys. Res. Lett., 49, e2022GL099317, https://doi.org/10.1029/2022gl099317, 2022.

Sang, J., Kim, M.-K., Lau, W. K. M., and Kim, K.-M.: Possible Impacts of snow darkening effects on the hydrological cycle over western Eurasia and east Asia, Atmosphere, 10, 500, https://doi.org/10.3390/atmos10090500, 2019.

Sarangi, C., Qian, Y., Rittger, K., Bormann, K. J., Liu, Y., Wang, H., Wan, H., Lin, G., and Painter, T. H.: Impact of light-absorbing particles on snow albedo darkening and associated radiative forcing over high-mountain Asia: high-resolution WRF-Chem modeling and new satellite observations, Atmos. Chem. Phys., 19, 7105–7128, https://doi.org/10.5194/acp-19-7105-2019, 2019.

Sarangi, C., Qian, Y., Rittger, K., Ruby Leung, L., Chand, D., Bormann, K. J., and Painter, T. H.: Dust dominates high-altitude snow darkening and melt over high-mountain Asia, Nat. Clim. Change, 10, 1045–1051, https://doi.org/10.1038/s41558-020-00909-3, 2020.

Schmale, J., Flanner, M., Kang, S. C., Sprenger, M., Zhang, Q. G., Guo, J. M., Li, Y., Schwikowski, M., and Farinotti, D.: Modulation of snow reflectance and snowmelt from Central Asian glaciers by anthropogenic black carbon, Scientific Reports, 7, 40501, https://doi.org/10.1038/srep40501, 2017.

Siegmund, A. and Menz, G.: Fernes nah gebracht – satelliten- und luftbildeinsatz zur analyse von umweltveränderungen im geographieunterricht, Geographie und Schule, 154, 2–10, 2005.

Shao, Y. and Dong, C. H.: A review on East Asian dust storm climate, modelling and monitoring, Global Planet. Change, 52, 1–22, https://doi.org/10.1016/j.gloplacha.2006.02.011, 2006.

She, J., Zhang, Y., Li, X., and Feng, X.: Spatial and temporal characteristics of snow cover in the Tizinafu watershed of the Western Kunlun Mountains, Remote Sens.-Basel, 7, 3426–3445, https://doi.org/10.3390/rs70403426, 2015.

Shi, T., Pu, W., Zhou, Y., Cui, J., Zhang, D., and Wang, X.: Albedo of black carbon-contaminated snow across Northwestern China and the validation with model simulation, J. Geophys. Res.-Atmos., 125, e2019JD032065, https://doi.org/10.1029/2019jd032065, 2020.

Shi, T., Cui, J., Chen, Y., Zhou, Y., Pu, W., Xu, X., Chen, Q., Zhang, X., and Wang, X.: Enhanced light absorption and reduced snow albedo due to internally mixed mineral dust in grains of snow, Atmos. Chem. Phys., 21, 6035–6051, https://doi.org/10.5194/acp-21-6035-2021, 2021.

Shi, T., Cui, J., Wu, D., Xing, Y., Chen, Y., Zhou, Y., Pu, W., and Wang, X.: Snow albedo reductions induced by the internal/external mixing of black carbon and mineral dust, and different snow grain shapes across northern China, Environ. Res., 208, 112670, https://doi.org/10.1016/j.envres.2021.112670, 2022a.

Shi, T., Chen, Y., Xing, Y., Niu, X., Wu, D., Cui, J., Zhou, Y., Pu, W., and Wang, X.: Assessment of the combined radiative effects of black carbon in the atmosphere and snowpack in the Northern Hemisphere constrained by surface observations, Environmental Science: Atmospheres, 2, 702–713, https://doi.org/10.1039/d2ea00005a, 2022b.

Shi, T., He, C., Zhang, D., Zhang, X., Niu, X., Xing, Y., Chen, Y., Cui, J., Pu, W., and Wang, X.: Opposite Effects of Mineral Dust Nonsphericity and Size on Dust-Induced Snow Albedo Reduction, Geophys. Res. Lett., 49, e2022GL099031, https://doi.org/10.1029/2022GL099031, 2022c.

Shi, Z., Xie, X., Li, X., Yang, L., Xie, X., Lei, J., Sha, Y., and Liu, X.: Snow-darkening versus direct radiative effects of mineral dust aerosol on the Indian summer monsoon onset: role of temperature change over dust sources, Atmos. Chem. Phys., 19, 1605–1622, https://doi.org/10.5194/acp-19-1605-2019, 2019.

Skiles, S. M. and Painter, T.: Daily evolution in dust and black carbon content, snow grain size, and snow albedo during snowmelt, Rocky Mountains, Colorado, J. Glaciol., 63, 118–132, https://doi.org/10.1017/jog.2016.125, 2016.

Skiles, S. M., Flanner, M., Cook, J. M., Dumont, M., and Painter, T. H.: Radiative forcing by light-absorbing particles in snow, Nat. Clim. Change, 8, 964–971, https://doi.org/10.1038/s41558-018-0296-5, 2018a.

Skiles, S. M., Mallia, D. V., Hallar, A. G., Lin, J. C., Lambert, A., Petersen, R., and Clark, S.: Implications of a shrinking Great Salt Lake for dust on snow deposition in the Wasatch Mountains, UT, as informed by a source to sink case study from the 13–14 April 2017 dust event, Environ. Res. Lett., 13, 124031, https://doi.org/10.1088/1748-9326/aaefd8, 2018b.

Sun, J., Zhang, M., and Liu, T.: Spatial and temporal characteristics of dust storms in China and its surrounding regions, 1960–1999: Relations to source area and climate, J. Geophys. Res.-Atmos., 106, 10325–10333, https://doi.org/10.1029/2000jd900665, 2001.

Tang, W., Dai, T., Cheng, Y., Wang, S., and Liu, Y.: A study of a severe spring dust event in 2021 over east Asia with WRF-Chem and multiple platforms of observations, Remote Sens.-Basel, 14, 3795, https://doi.org/10.3390/rs14153795, 2022.

Teillet, P. M., Guindon, B., and Goodenough, D. G.: On the slope-aspect correction of multispectral scanner data, Can. J. Remote Sens., 8, 84–106, https://doi.org/10.1080/07038992.1982.10855028, 1982.

Thakur, R. C., Arun, B. S., Gogoi, M. M., Thamban, M., Thayyen, R. J., Redkar, B. L., and Suresh Babu, S.: Multi-layer distribution of Black Carbon and inorganic ions in the snowpacks of western Himalayas and snow albedo forcing, Atmos. Environ., 261, 118564, https://doi.org/10.1016/j.atmosenv.2021.118564, 2021.

Usha, K. H., Nair, V. S., and Babu, S. S.: Deciphering the role of aerosol-induced snow albedo feedback on dust emission over the Tibetan Plateau, J. Geophys. Res.-Atmos., 127, e2021JD036384, https://doi.org/10.1029/2021jd036384, 2022.

Wake, C. P., Mayewski, P. A., Li, Z., Han, J., and Qin, D.: Modern eolian dust deposition in central Asia, Tellus B, 46, 220–233, https://doi.org/10.3402/tellusb.v46i3.15793, 1994.

Wang, X., Huang, J., Ji, M., and Higuchi, K.: Variability of East Asia dust events and their long-term trend, Atmos. Environ., 42, 3156–3165, https://doi.org/10.1016/j.atmosenv.2007.07.046, 2008.

Wang, X., Doherty, S. J., and Huang, J.: Black carbon and other light-absorbing impurities in snow across Northern China, J. Geophys. Res.-Atmos., 118, 1471–1492, https://doi.org/10.1029/2012jd018291, 2013.

Wang, X., Pu, W., Ren, Y., Zhang, X., Zhang, X., Shi, J., Jin, H., Dai, M., and Chen, Q.: Observations and model simulations of snow albedo reduction in seasonal snow due to insoluble light-absorbing particles during 2014 Chinese survey, Atmos. Chem. Phys., 17, 2279–2296, https://doi.org/10.5194/acp-17-2279-2017, 2017.

Wang, X., Wei, H., Liu, J., Xu, B., Wang, M., Ji, M., and Jin, H.: Quantifying the light absorption and source attribution of insoluble light-absorbing particles on Tibetan Plateau glaciers between 2013 and 2015, The Cryosphere, 13, 309–324, https://doi.org/10.5194/tc-13-309-2019, 2019.

Wei, T., Dong, Z., Kang, S., Qin, X., and Guo, Z.: Geochemical evidence for sources of surface dust deposited on the Laohugou glacier, Qilian Mountains, Appl. Geochem., 79, 1–8, https://doi.org/10.1016/j.apgeochem.2017.01.024, 2017.

Wiscombe, W. J. and Warren, S. G.: A model for the spectral albedo of snow. I. Pure snow, J. Atmos. Sci., 37, 2712–2733, https://doi.org/10.1175/1520-0469(1980)037<2712:AMFTSA>2.0.CO;2, 1980.

Wu, D., Liu, J., Wang, T., Niu, X., Chen, Z., Wang, D., Zhang, X., Ji, M., Wang, X., and Pu, W.: Applying a dust index over North China and evaluating the contribution of potential factors to its distribution, Atmos. Res., 254, 105515, https://doi.org/10.1016/j.atmosres.2021.105515, 2021.

Wu, G., Yao, T., Xu, B., Tian, L., Zhang, C., and Zhang, X.: Dust concentration and flux in ice cores from the Tibetan Plateau over the past few decades, Tellus B, 62, 197–206, https://doi.org/10.1111/j.1600-0889.2010.00457.x, 2010.

Xu, J., Kang, S., Hou, S., Zhang, Q., Huang, J., Xiao, C., Ren, J., and Qin, D.: Characterization of contemporary aeolian dust deposition on mountain glaciers of western China, Sci. Cold Arid Reg., 8, 9–21, https://doi.org/10.3724/SP.J.1226.2016.00009, 2016.

Yang, L., Shi, Z., Xie, X., Li, X., Liu, X., and An, Z.: Seasonal changes in East Asian monsoon-westerly circulation modulated by the snow-darkening effect of mineral dust, Atmos. Res., 279, 106383, https://doi.org/10.1016/j.atmosres.2022.106383, 2022.

Yao, T., Thompson, L., Yang, W., Yu, W., Gao, Y., Guo, X., Yang, X., Duan, K., Zhao, H., Xu, B., Pu, J., Lu, A., Xiang, Y., Kattel, D. B., and Joswiak, D.: Different glacier status with atmospheric circulations in Tibetan Plateau and surroundings, Nat. Clim. Change, 2, 663–667, https://doi.org/10.1038/nclimate1580, 2012.

Yao, T., Xue, Y., Chen, D., Chen, F., Thompson, L., Cui, P., Koike, T., Lau, W. K. M., Lettenmaier, D., Mosbrugger, V., Zhang, R., Xu, B., Dozier, J., Gillespie, T., Gu, Y., Kang, S., Piao, S., Sugimoto, S., Ueno, K., Wang, L., Wang, W., Zhang, F., Sheng, Y., Guo, W., Ailikun, Yang, X., Ma, Y., Shen, S. S. P., Su, Z., Chen, F., Liang, S., Liu, Y., Singh, V. P., Yang, K., Yang, D., Zhao, X., Qian, Y., Zhang, Y., and Li, Q.: Recent Third Pole's rapid warming accompanies cryospheric melt and water cycle intensification and interactions between monsoon and environment: Multidisciplinary approach with observations, modeling, and analysis, B. Am. Meteorol. Soc., 100, 423–444, https://doi.org/10.1175/bams-d-17-0057.1, 2019.

Yao, T., Bolch, T., Chen, D., Gao, J., Immerzeel, W., Piao, S., Su, F., Thompson., L., Wada, Y., Wang, L., Wang, T., Wu, G., Xu, B., Yang, W., Zhang, G., and Zhao, P.: The imbalance of the Asian water tower, Nature Reviews Earth & Environment, 3, 1–15, https://doi.org/10.1038/s43017-022-00299-4, 2022.

Yuan, T., Chen, S., Huang, J., Wu, D., Lu, H., Zhang, G., Ma, X., Chen, Z., Luo, Y., and Ma, X.: Influence of dynamic and thermal forcing on the meridional transport of Taklimakan desert dust in spring and summer, J. Climate, 32, 749–767, https://doi.org/10.1175/jcli-d-18-0361.1, 2018.

Zege, E. P., Katsev, I. L., Malinka, A. V., Prikhach, A. S., Heygster, G., and Wiebe, H.: Algorithm for retrieval of the effective snow grain size and pollution amount from satellite measurements, Remote Sens. Environ., 115, 2674–2685, https://doi.org/10.1016/j.rse.2011.06.001, 2011.

Zhang, B., Tsunekawa, A., and Tsubo, M.: Contributions of sandy lands and stony deserts to long-distance dust emission in China and Mongolia during 2000–2006, Global Planet. Change, 60, 487–504, https://doi.org/10.1016/j.gloplacha.2007.06.001, 2008.

Zhang, X., Li, Z. Q., You, X. N., She, Y. Y., Song, M. Y., and Zhou, X.: Light-Absorbing Impurities on Urumqi

Glacier No. 1 in Eastern Tien Shan: Concentrations and Implications for Radiative Forcing Estimates During the Ablation Period, Frontiers in Earth Science, 9, 2296–6463, https://doi.org/10.3389/feart.2021.524963, 2021.

Zhang, Y., Kang, S., Sprenger, M., Cong, Z., Gao, T., Li, C., Tao, S., Li, X., Zhong, X., Xu, M., Meng, W., Neupane, B., Qin, X., and Sillanpää, M.: Black carbon and mineral dust in snow cover on the Tibetan Plateau, The Cryosphere, 12, 413–431, https://doi.org/10.5194/tc-12-413-2018, 2018.

Zhang, Y., Gao, T., Kang, S., Sprenger, M., Tao, S., Du, W., Yang, J., Wang, F., and Meng, W.: Effects of black carbon and mineral dust on glacial melting on the Muz Taw glacier, Central Asia, Sci. Total Environ., 740, 140056, https://doi.org/10.1016/j.scitotenv.2020.140056, 2020.

Zhang, Y., Gao, T., Kang, S., Shangguan, D., and Luo, X.: Albedo reduction as an important driver for glacier melting in Tibetan Plateau and its surrounding areas, Earth-Sci. Rev., 220, 103735, https://doi.org/10.1016/j.earscirev.2021.103735, 2021.

Zhao, X., Huang, K., Fu, J. S., and Abdullaev, S. F.: Long-range transport of Asian dust to the Arctic: identification of transport pathways, evolution of aerosol optical properties, and impact assessment on surface albedo changes, Atmos. Chem. Phys., 22, 10389–10407, https://doi.org/10.5194/acp-22-10389-2022, 2022.

Zhu, L., Ma, G., Zhang, Y., Wang, J., Tian, W., and Kan, X.: Accelerated decline of snow cover in China from 1979 to 2018 observed from space, Sci. Total Environ., 814, 152491, https://doi.org/10.1016/j.scitotenv.2021.152491, 2022.